Ⅲ-4

Surface, Interface and Thin Films

Highlight

BL3U

In-situ O K-edge XAFS Measurements of MnO_x Oxygen Evolution Catalysts Containing Alkali Metal Cations

M. Yoshida[1, 2], F. Yamamoto[1], M. Nagasaka[3], H. Yuzawa[3], N. Kosugi[3] and H. Kondoh[1]

[1]*Department of Chemistry, Keio University, Yokohama 223-8522, Japan*

[2]*Cooperative Research Fellow, Institute for Catalysis, Hokkaido University, Sapporo 001-0021, Japan*

[3]*Institute for Molecular Science, Okazaki 444-8585, Japan*

Electrochemical hydrogen production from water using renewable energy attracts attention to construct a sustainable society. For this purpose, electrocatalysts for hydrogen and oxygen evolution reactions (HER and OER, respectively) are used to decompose water ($2H_2O \rightarrow 2H_2+O_2$). However, the efficiency of OER is insufficient compared with that of HER. Thus, the development of efficient OER catalysts has been required to improve the activity for overall water splitting. In this situation, the layered manganese oxide containing K^+ cation (K:MnO_x) was reported to function as an efficient catalyst for OER over a wide pH range [1]. Meanwhile, we found that the OER activity of the layered Mn oxide is enhanced when Cs^+ cation is contained in the catalysts (Cs:MnO_x). Therefore, in this study, we investigated the reaction mechanism of M:MnO_x (M = Na, K, Cs) catalysts by in-situ O K-edge X-ray absorption fine structure (XAFS) measurements under potential control conditions and discussed the effect of cations in the catalysts.

Electrochemical O K-edge XAFS measurements with transmission mode using soft X-rays were performed at BL3U in the UVSOR Synchrotron, according to the previous works [2]. A home-made electrochemical cell was used with Au/Cr/SiC thin film substrates as working electrodes, a Pt counter electrode, and a Ag/AgCl reference electrode. The Na:MnO_x, K:MnO_x, and Cs:MnO_x catalysts were electrodeposited on the Au/Cr/SiC working electrode at 0.6 V in methylphosphonate electrolyte containing $MnCl_2$ and XOH (X = Na, K, and Cs, respectively).

Prior to the O K-edge XAFS, in-situ Mn K-edge XAFS measurements were tested for the Na:MnO_x, K:MnO_x, and Cs:MnO_x. The results exhibited that the manganese species in the catalysts were present as Mn^{3+} with δ-MnO_2 structure at lower electrode potential and as Mn^{4+} with δ-MnO_2 structure at higher electrode potential. In addition, the estimation of manganese valence suggested that the fraction of Mn^{3+} species in the Cs:MnO_x under OER condition was higher than those in the Na:MnO_x and K:MnO_x.

Next, the in-situ O K-edge XAFS spectra for Na:MnO_x, K:MnO_x, and Cs:MnO_x were taken under electrode potential control in a phosphate buffered electrolyte, as shown in Figure 1. An absorption peak was observed around 529 eV at 0.0 and 1.0 V for all catalysts. From the comparison with reference samples, it was found that the absorption peak was attributed to the δ-MnO_2, consistent with the results of Mn K-edge XAFS. However, even if the electrode potential was changed from 0.0 to 1.0 V, the O K-edge XAFS spectra did not change so much, meaning that the electronic states of oxygen species in the δ-MnO_2 structure were almost the same between lower and higher electrode potentials. On the other hand, a peak of higher energy around 531.8 eV was slightly disordered for Cs:MnO_x compared with Na:MnO_x and K:MnO_x, indicating that the larger amount of hydroxide or hydroxyl group may be generated for Cs:MnO_x, in response to the presence of Mn^{3+} species.

In conclusion, we measured in-situ O K-edge XAFS for M:MnO_x catalysts and revealed that the chemical state of M:MnO_x was δ-MnO_2 under OER condition. The presence of Mn^{3+} species in the Cs:MnO_x is likely to be the key of OER activity.

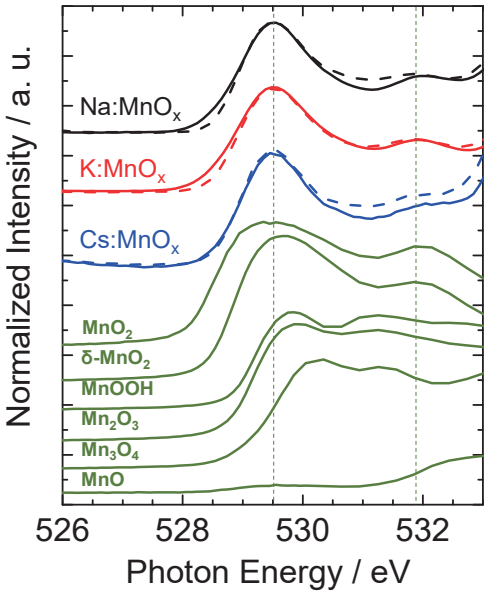

Fig. 1. In-situ O K-edge XAFS spectra of Na:MnO_x, K:MnO_x, Cs:MnO_x electrocatalysts at 1.0 V (solid line) and 0.0 V (dotted line) in phosphate buffered electrolyte.

[1] (a) D. G. Nocera *et al.*, J. Am. Chem. Soc. **136** (2014) 6002. (b) J. Am. Chem. Soc. **137** (2015) 14887.
[2] (a) M. Nagasaka *et al.*, J. Phys. Chem. C **117** (2013) 16343. (b) M. Yoshida *et al.*, J. Phys. Chem. C **119** (2015) 19279.

BL2A

Studies on Interface of Thin Film by Near-edge X-ray Absorption Fine Structure

E. Kobayashi[1], K. K. Bando[2], O. Takahashi[3], K. K. Okudaira[4] and T. Okajima[1]

[1]*Kyushu Synchrotron Light Research Center, Tosu 841-0005, Japan*

[2]*National Institute of Advanced Industrial Science and Technology, Tsukuba 305-8565, Japan*

[3]*Institute for Sustainable Science and Development, Hiroshima University, Higashi-Hiroshima 739-8526, Japan*

[4] *Chiba University, Chiba 263-8522, Japan*

Resistive random access memory (ReRAM) is expected as a new next generation memories. The memory operates by applying a voltage to a structure in which an oxide film is sandwiched between electrodes. However, the mechanism of action and degradation mechanism have not been clarified yet. It is important to investigate the metal/oxide interface to elucidate them. Near-edge X-ray absorption fine structure (NEXAFS) is effective as one of methods to investigate the change in chemical state and depth profiling of the film. In this paper, we investigated the interface of Al/SiO_2/Si(111) by NEXAFS.

The silicon oxide thin films (~3ML) prepared on Si(111) using molecular beam epitaxy (MBE). Si *K*-edge NEXAFS spectra of thin film were measured at the beamline 2A of the UVSOR. The experimental setup for NEXAFS measurement is shown in Fig. 1. The soft x-ray was passed through a metal mesh and was irradiated to the sample. In the total electron yield (TEY), the drain current of the sample was measured. The fluorescence from sample was detected by silicon drift detectors. Potential of the sample was applied between the metal mesh and metal plate. All experiments were performed at room temperature.

Figure 2 shows the Si *K*-edge NEXAFS spectra of Al/SiO_2/Si(111) obtained from partial fluorescence yield (PFY) and TEY mode.

The spectra of TEY mode show a strong peak at around 1847 eV. The spectral features are similar to that of bulk SiO_2. Although the overall structure of the spectrum has hardly changed before and after discharging, the peak intensity of spectrum after discharging became weak. This indicates that interaction occurs at the interface between Al and SiO_2 by voltage application.

The peak of the spectrum in the PFY mode was observed on the lower energy side than in the TEY mode. The spectrum peak of bulk Si is observed at about 1840 eV. Therefore the origin of the observed peak is near the SiO_2/Si interface. The intensity changed when a potential was applied. This indicates that the silicon oxide changed due to voltage application.

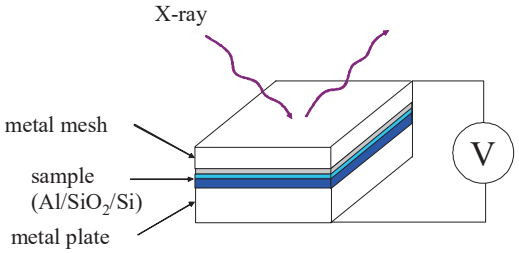

Fig. 1. experimental setup.

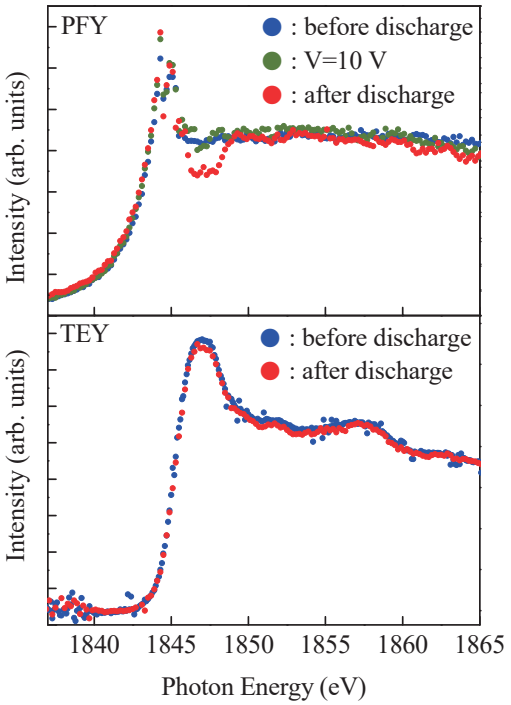

Fig. 2. Si *K*-edge NEXAFS spectra of Al/SiO_2/Si(111) obtained from PFY and TEY mode.

BL2A

Studies on Chemical State of Oxide Film under Applied Voltage by Near-edge X-ray Absorption Fine Structure

K. K. Okudaira[1], O. Takahashi[2], K. K. Bando[3] and E. Kobayashi[4]

[1] *Chiba University, Chiba 263-8522, Japan*

[2]*Institute for Sustainable Science and Development, Hiroshima University, Higashi-Hiroshima 739-8526, Japan*

[3]*National Institute of Advanced Industrial Science and Technology, Tsukuba 305-8565, Japan*

[4]*Kyushu Synchrotron Light Research Center, Tosu 841-0005, Japan*

High-k aluminum oxide (Al_2O_3) is considered a potential alternative gate dielectric material on Si substrates for application to not only conventional inorganic transistor but also organic filed-effect transistors (OTFT). In particular, OTFT have been the focus of considerable research activity during the past 10 years [1]. The performance of OTFT depends critically on the use of high-performance dielectrics that form active interfaces with low defect densities. In principle, for a given thickness of dielectric, a high-*k* dielectric is preferable to a low-k dielectric for an FET application that requires the FET to exhibit a high drive current at low drive voltage. Various solution-processible high-*k* dielectrics for low-voltage OFET have been used such as anodized aluminum oxide (dielectric constant = 8–10) [2]. The charge injection efficiency depends on energy level alignment of the interface between the dielectrics surface and the organic semiconductor layer. The surface Al_2O_3 is strongly influenced by the degree of surface hydroxylation [3].

In this paper, we investigated the chemical state of an Al_2O_3 under applied voltage by NEXAFS.

An alumina film was made on a polished stainless steel plate by dip-coating with a diluted alumina sol (Kawaken Fine Chemicals, F1000). The coated plate was dried at 333 K, 6 hours and calcined at 473 K, 3 hours in an oven.

Al *K*-edge NEXAFS spectra of aluminum oxide thin film were measured at the beamline 2A of the UVSOR. The soft x-ray was passed through a metal mesh and was irradiated to the sample. The fluorescence from sample was detected by silicon drift detectors. Potential of the sample was applied between the metal mesh and metal plate. All experiments were performed at room temperature.

Figure 1 shows the Al *K*-edge NEXAFS spectra of aluminum oxide obtained from PFY mode at various applied voltage. The spectra were measured while applying a voltage. This sample caused breakdown at ~ 0.8 V. After breakdown, the potential to the sample could not be applied. The spectra show a strong peak at around ~1568 eV, attributed to Al bonded to OH group in the Al_2O_3 film. Although the overall structure of the spectrum has hardly changed, the intensity of the main peak decreases as applied voltage becomes higher. Furthermore, after discharge the intensity of the main peak does not turn back to that at V = 0 V This indicates that the application of voltage affect the structure of the Al-OH moiety in the film.

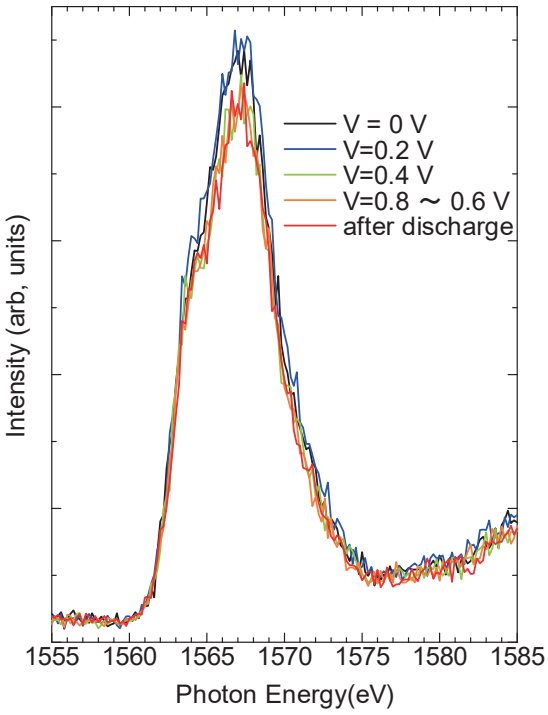

Fig. 1. Al *K*-edge NEXAFS spectra of aluminum oxide thin film obtained from PFY mode at various applied voltage.

[1] H. Sirringhaus, Adv. Mater. **17** (2005) 2411.
[2] L. A. Majewski, M. Grell, S. D. Ogier and J. Veres, Org. Electron. **4** (2003) 27.
[3] P. J. Eng, T. P. Trainor, G. E. Brown Jr., G. A. Waychunas, M. Newville, S. R. Sutton and M. L. Rivers, Science **288** (2000) 1029.

BL2B

Modification of the Overlapping of the Frontier Orbitals

Y. Yamada[1], Y. Hasegawa[1], T. Maeda[1], T. Hosokai[2] and K. R. Koswattage[3]
[1]*Institute of Applied Physics, University of Tsukuba, Tsukuba 305-8573, Japan*
[2]*National Institute of Advanced Industrial Science and Technology, Tsukuba 305-8568, Japan*
[3]*Institute for Molecular Science, Department of Photo-Molecular Science, Okazaki 444-8585, Japan*

Organic semiconductors with enhanced intermolecular interaction have attracted attentions since they may exhibit an enhanced intermolecular overlapping of the frontier orbitals and thus the band-like transport. By tailoring unique ordering of these molecules on the well defined substrate, we are able to modify the intermolecular overlapping of the frontier orbitals, resulting in significant alteration of the electronic states from that of the bulk. In this study, we focused on simple examples of these molecules such as DNTT and sumanene.

In order to realize the control of molecular packing and electronic structure of these molecules in a realistic environment, all the experiments were done at room temperature. ARPES measurements are done in BL2B of UVSOR with the incident light of 28 eV.

[1. DNTT on Ag(110)]

We have shown that, there exist two types of ordering of the monolayer of DNTT, i.e, the dense phase and the loose phase, and that the dense packing induces a considerable splitting of HOMO due to overlapping [1]. Recently, we found that the one-dimensional structure of the "loose" DNTT monolayer can be formed on the anisotropic Ag(110) substrate (Fig. 1 (a)). The monolayer consists of apparent molecular rows; the long axis of molecules in the row is parallel to the direction of the rows.

In the ARPES spectra obtained along the direction of the molecular rows, i.e, parallel to the molecular axis (Fig. 1 (b)), the intra-molecule dispersion-like feature was observed, similarly to the case of well-ordered pentacene [2] or 6P [3]. The intramolecule dispersion apparently exhibits a backfolding due to the periodicity of half-length of the molecule, possibly reflecting the characteristic molecular shape. On the other hand, in the perpendicular to the row, i.e, perpendicular to the molecular axis, each orbitals show almost negligible band dispersion, suggesting that the intermolecule overlapping is small because of the loose packing in this structure, in contrast to our previous observation in the dense monolayer of DNTT [1]. Therefore, we note that the band dispersion in this type of system does not necessarily reflect the band dispersion of the bulk system.

[2. Sumanene/Cu(111)]

Sumanene on Au(111) and Ag(111) are found to take a flat-lying geometry with the bowl-up and bowl-down molecules [4]. On the other hand, Sumanene monolayer on Cu(111) exhibit one-dimensional stacking of slightly-tilted sumanene molecules (Fig. 2 (a)). The monolayer consists of the five different rows of sumanene.

The ARPES spectrum along the molecular rows is shown in Fig. 2 (b). The molecular orbitals are broad because of the presence of five bands. Although enhanced π-stacking in the molecular row is expected, we found almost no apparent dispersion in the upper frontier orbitals such as HOMO and HOMO-1. On the other hand, weak dispersing feature is seen in the lower-lying orbitals which is not seen in the ARPES spectrum taken perpendicular to the row. The detailed calculation is ongoing in order to determine the orbitals responsible to the observed dispersion.

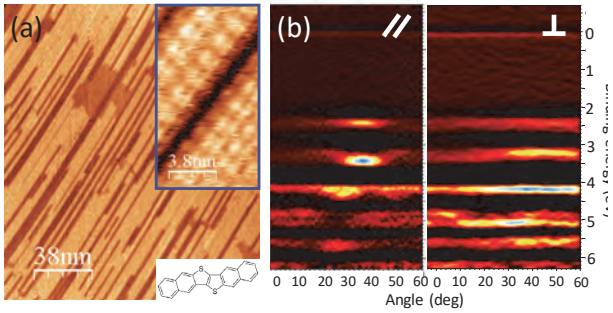

Fig. 1. (a) STM image of several layer of DNTT/Ag (110). (b) ARUPS along and perpendicular to the molecular axis.

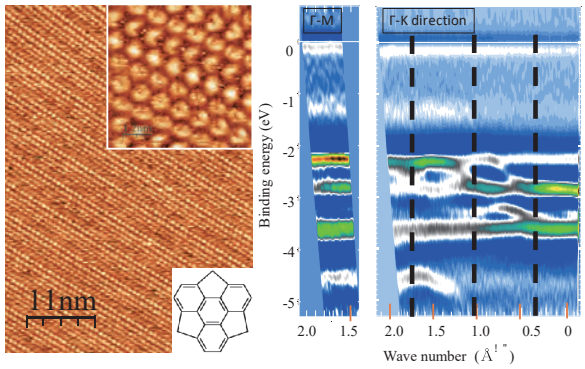

Fig. 2. (a) STM image of monolayer of sumanene/cu (111). (b) ARUPS along and perpendicular to the molecular row.

[1] Y. Hasegawa *et al.*, J. Phys. Chem. C, **120** (2016) 21536.
[2] S.Berkebile, *et al.*, Phys. Rev. B **77** (2008) 115312.
[3] G. Koller, *et al.*, Science **317** (2007) 351.
[4] Y. Yamada, (in preperation).

BL2B

ARUPS of Pentacene on a-TES Film Prepared on SiO_2

Y. Urabe[1], Y.Aoki[2] and K. K. Okudaira[1]
[1]*Association of Graduate Schools of Science and Technology, Chiba University,Chiba 263-8522, Japan*
[2]*Faculty of Engineeringy, Chiba University, Chiba 263-8522, Japan*

An organic thin-film transistor (OTFT) has been actively studied in recent years. To achieve high mobility it is important to improve the charge injection efficiency at the interface between the substrate and the organic semiconductor layer and charge transfer probability. Self-assembled monolayers (SAMs) has been introduced on metal electrode and insulator layer in order to arrange the molecular orientation of organic semiconductor film and energy level alignment of the interface [1].

For the case of a bottom-contact type OTFT, it is necessary to introduce two kinds of SAM chemically bonded to not only metal electrode but also insulator layer. A triazine-based molecular adhesion agent (a-TES : 6-triethoxysilyl propylamino-1,3,5- triazine-2,4-dithiol(TES)) was used for preparing thin film like self-assembly monolayers on Cu surface as well as SiO_2 insulator layer

In this work we used a-TES modified SiO_2 substrate and examined the molecular orientation of pentacene thin films thermally deposited on the surface by angle-resolved ultraviolet photoelectron spectroscopy (ARUPS) measurements. To obtain the quantitative analysis on the molecular orientation; we compare observed take-off angle dependence of π band and calculated ones by the independent-atomic-center (IAC)/MO approximation [2].

ARUPS measurements were performed at the beam line BL2B of the UVSOR. The take-off angle (θ) dependencies of photoelectron spectra were measured with the photon energy (hν) of 28 eV. We use a-TES modified SiO_2 and SiO_2 as substrate. SiO_2 substrate was subjected to ultrasonic cleaning for 10 minutes in acetone, isopropanol, and then ozone cleaning for 30 minutes. a-TES modified SiO_2 substrate was obtained by dipped in 0.1% solution at 20°C for 30 minutes. Pentacene was deposited on 1.4 nm on both substrates.

We observed take-off angle (θ) dependence of HOMO peak in UPS of pentacene deposited on a-TES/SiO_2 and SiO_2 (thickness of 1.4 nm).

The HOMO peaks of pentacene on a-TES/SiO_2 and on SiO_2 appear at binding energy of about 1 eV and 2eV, respectively. The HOMO peaks of pentacene both on a-TES/SiO_2 and on SiO_2 show intense peaks at higher take-off angle (θ = 60°), and at lower θ these intensities become small. For a-TES/SiO_2, HOMO intensity at θ = 20° is smaller than that at θ = 0°. On the other hand, for SiO_2 substrate, HOMO intensity at θ = 20° is almost same as that at θ = 0°. Due to the difference of θ dependence of HOMO peak on a-TES/SiO_2 and on SiO_2, it is found that the molecular orientation of pentacene on a-TES/SiO_2 is different from that on SiO_2. The difference of surface energy of a-TES and SiO_2 indicates that the surface modification by a-TES affects the molecular orientation of organic semiconductor layer, which would have an effect on the characteristics of OTFT such as mobility.

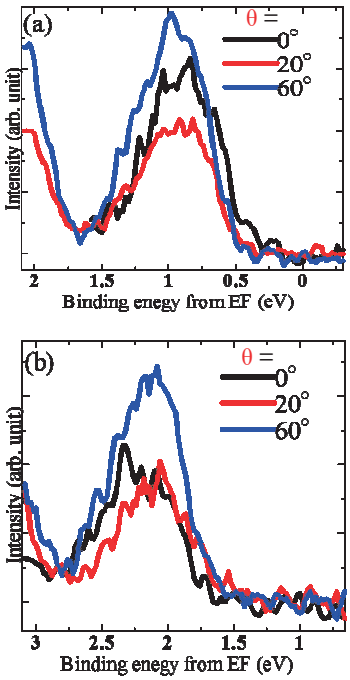

Fig. 1. ARUPS of pentacene(1.4nm)/SiO_2 (a) and pentacen(1.4nm)/a-TES/SiO_2 (b).

[1] F. Wang *et al*., Nanoscale Res. Lett. **6** (2011) 483.
J. –P. Hong *et al*., Appl. Phys. Lett. **92** (2008) 143311.
[2] N. Ueno *et al*., J. Chem. Phys. **99** (1993) 7169.

BL2B

Electronic States of Self-assembled Peptide Films on the Graphite Surface

Y. Nakayama[1], T. Narimatsu[2] and Y. Hayamizu[2, 3]

[1]*Faculty of Science and Technology, Tokyo University of Science, Noda 278-8510, Japan*
[2]*Department of Materials Science and Engineering, Tokyo Institute of Technology, Tokyo 152-8550, Japan*
[3]*PRESTO, Japan Science and Technology Agency (JST), Kawaguchi 332-0012, Japan*

One promising route for bioelectronics and biosensing is functionalization of electrodes by proteins such as enzymes and antibodies. Therefore, attachment of the protein molecules onto the electrode surfaces is a crucial problem. Thiol groups of the cysteine residues can be utilized as "anchors" for binding the protein molecule covalently onto the noble metal electrodes, whose interface properties our group has already reported so far [1]. Besides these conventional electrode materials, graphene is attracting growing interests due to its biocompatibility. On the graphene or graphite, benzene rings of some amino residues (such as tyrosine) preferentially adsorb on the surface through the π-π interaction.

Recently, peptides, fragments of proteins, of certain sequences are discovered to build regular networked structures spontaneously on the graphite surface [2]. Some of these peptide molecules dope the graphene electric devices to switch the transport properties [3], yet the electronic origins of such functionalities are still unsolved. In the present study, we examined the interface electronic structures between a functional peptide GrBP5-WT [2] and the graphite surface.

Self-assembled peptide film samples were prepared by procedures described elsewhere [2, 3]. Ultraviolet photoelectron spectroscopy (UPS) measurements were conducted at BL2B of UVSOR.

Figure 1 (a) shows UPS spectra of submonolayer and multilayer films of the peptide. The profile of the latter is fairly consistent to simulated density-of-states (DOS) curve based on quantum-chemical calculation results for the whole GrBP5-WT molecule, while that of the former rather resembles the DOS of the left-half fragment of this peptide molecule. Taking into consideration that the anchoring groups on graphite are tyrosine (Y) residues in the right-half of this peptide, this changing tendency of the UPS profiles implies disordering in the molecular orientation from the first adsorbed layer to the multilayers. The UPS spectra of the highest-occupied molecular orbital (HOMO) and secondary-electron cutoff (SECO) regions are shown in Figs. 1 (b) and (c), respectively. From the low-energy onset position of the HOMO and work function value derived from the SECO spectra, the ionization energy of this peptide is determined to be 7.6 eV. A rise in the work function by formation of the GrBP5-WT film indicates electron transfer from graphite to the overlayer, which rationalizes the reported functionality of this peptide as an acceptor for the graphene devices [3].

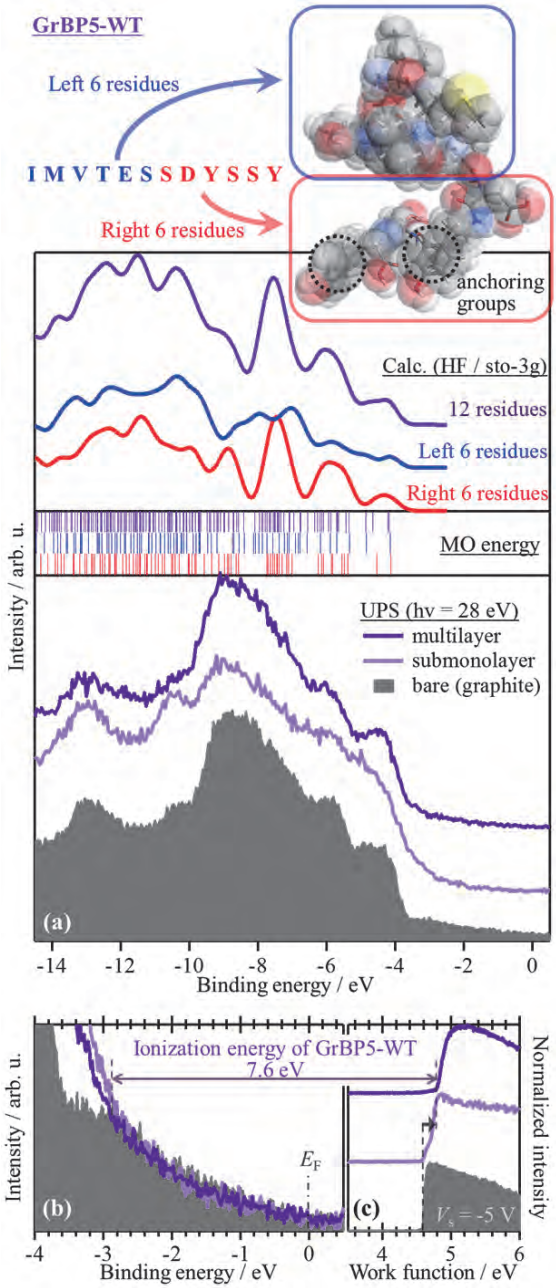

Fig. 1. (a-c) UPS spectra of self-assembled peptide GrBP5-WT (upper inset) films on graphite substrates. Simulated DOS distributions and molecular orbital (MO) energies are also displayed in (a).

[1] K. R. Koswattage *et al*., e-J. Surf. Sci. Nanotechnol. **13** (2015) 373; *idem*, UVSOR Activity Reports **40** (2013) 90.
[2] C. R. So *et al*., ACS Nano **6** (2012) 1648.
[3] Y. Hayamizu *et al*., Sci. Rep. **6** (2016) 33778.

BL2B

Electronic Structures of Organic-Metal Interface Measuring by UPS: bis(l,2,5-thiadiazolo)-p-quinobis(l,3-dithiole) and Tris-(8-hydroxyquinoline)aluminum Alq3

N. Ohashi[1], S. Kobayashi[1], M. Hikasa[2], Y. Nakayama[2] and Y. Watanabe[1]

[1]*Department of Electrical and Electronic Engineering, Faculty of Engineering, Tokyo University of Science, Chino 391-0292, Japan*

[2]*Department of Pure and Applied Chemistry, Faculty of Science and Technology, Tokyo University of Science, Noda 278-8510, Japan*

In this report, we were investigated two types of metal-organic interface. First one is bis (l, 2, 5-thiadiazolo)-p-quinobis (l, 3-dithiole) (BTQBT)-aluminum interface. BTQBT was known as high performance organic semiconductor which shows maximum mobility of 4 cm^2/Vs. [1] A vertical type transistors with BTQBT shows current density of 1 A/cm^2 and on/off current ratio of over 10^5. [2] These reports prove a superiority of BTQBT, however, device operation mechanism of the vertical-type transistor is still unclear. So we investigate BTQBT and aluminum interface by ultraviolet photoelectron spectroscopy (UPS) at the first of the research.

The UPS measurement was performed at BL2B of UVSOR. Photon energy was 38 eV. We have prepared Si substrate covered with gold film. Aluminum and BTQBT were fabricated on the substrates by vacuum deposition. All experiments were carried out in vacuo.

Figure 1 shows UPS spectra of BTQBT on aluminum electrode. BTQBT thickness dependence with UPS spectra was examined for the purpose of estimating the energy level diagram of BTQBT-aluminum interface. The UPS results of SECO position indicates that the vacuum level varies with thickness of BTQBT. The vacuum level shift of the bulk region correspond to the HOMO edge of BTQBT shown in Fig. 1 (b). It is attributed band bending of BTQBT. We summarized vacuum level shift of BTQBT film in Fig. 2. The Vacuum level is abruptly changed at the very interface of BTQBT and aluminum. The vacuum level is stable near the interface, then varies with thickness at the bulk region. The charge injection barrier of BTQBT-aluminum interface was estimated 0.78 eV.

Next then, we briefly explained second topic, Alq3-PEI-ITO interface. (Alq3 and PEI stand for Tris-(8-hydroxyquinoline)aluminum and poly ethylene imine, respectively.) Recently, it was reported that ITO covered with ultrathin PEI performed excellent electron injection layer. [3] We investigated electronic structure of Alq3-PEI-ITO interface by UPS. Figure 3 shows UPS spectra of Alq3. Energy level of the Alq3 spectrum was shifted to low kinetic energy side, and there was no interface state. It suggest that vacuum level shift (0.5 eV) by PEI partly diminished electron injection barrier (1.5 eV). The electron injection mechanism of PEI is still under investigation.

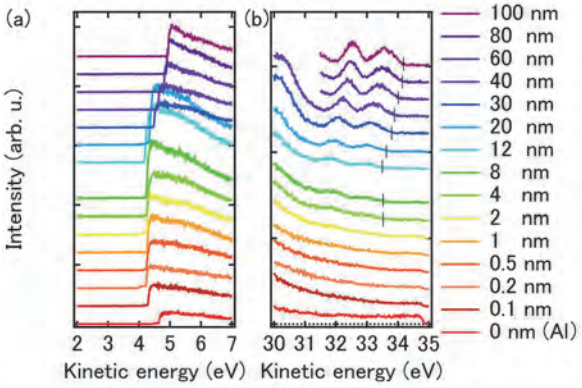

Fig. 1. Photo emission spectra of BTQBT on Al interface. (a) the secondary electron cut-off (SECO) position (b) the Fermi edge position. Black solid lines indicates HOMO edge of BTQBT.

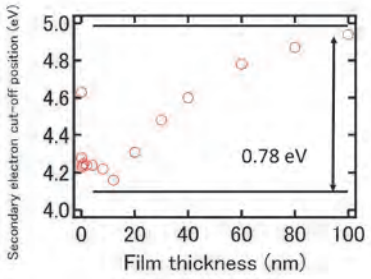

Fig. 2. SECO vs film thickness of BTQBT.

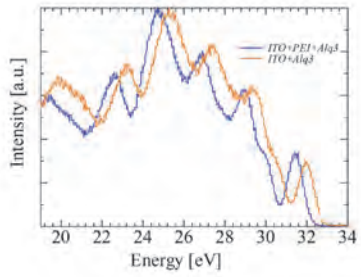

Fig. 3. UPS spectra of Alq3 on ITO interface, with and without PEI ultrathin layer.

[1] S. Hasegawa, *et al*., J. Chem. Phys. **100** (1994) 6969.
[2] H. Fukagawa, Y. Watanabe, *et al.*, AIP Advance **6** (2016) 045010.
[3] H. Fukagawa *et al*., APEX **7** (2014) 082104.

BL3B

Oxygen Vacancy in Solution-processed IGZO Thin-Film Transistors and Its Effect on Transistor Characteristics

Y. Ochiai[1], T. Morimoto[1], N. Fukuda[3] and Y. Ohki[1,2]

[1]*Waseda University, Tokyo 169-8555, Japan*

[2]*Research Institute for Materials Science and Technology, Waseda University, Tokyo 169-8555, Japan*

[3]*Flexible Electronics Research Center (FLEC), National Institute of Advanced Industrial Science and Technology (AIST), Tsukuba 305-8565, Japan*

Using a solution process, by which films can be produced at low cost, we have successfully made IGZO thin-film transistors (TFTs) with a mobility of 5.1 cm^2/Vs, which is higher than that of amorphous Si TFTs [1]. In this paper, the transfer characteristics of these TFTs are studied, focusing on the effects of oxygen vacancy, Ga content, and sintering temperature.

Six precursor solutions of IGZO were prepared by dissolving each nitrate of In, Ga, or Zn with a molar ratio of 1:*x*:1 (*x*: 0 to 8) in 2-methoxyethanol. The solution was spin-coated on a 300-nm thick thermally oxidized SiO_2 on a p-type silicon substrate and sintered at 300 or 800 °C for 1 hour in air. Then, Al was vacuum-evaporated on the film to form a drain electrode and a source electrode, by which we obtained a TFT with a gate length of 50 μm and a width of 500 μm. Next, its transfer characteristics were measured by raising the gate voltage applied to the substrate from -40 to +80 V, while the source electrode was earthed and the drain electrode was biased to +40 V dc.

The inset in Fig. 1 shows the drain current as a function of gate voltage, while Fig. 1 shows the relation between the on-current (I_D at V_G = 80 V) obtained from the transfer characteristics and the Ga content. For the films sintered at 300°C, the on-current decreases monotonically with the increase in Ga content, whereas it becomes maximum at the Ga content of 40% in the films sintered at 800°C.

The inset in Fig. 2 shows an XPS spectrum of O1s electrons observed in an IGZO film with a Ga content of 0% sintered at 300°C and its three components at 530 eV due to oxygen bonding with metal, at 531 eV due to oxygen adjacent to oxygen vacancies (V_O), and at 532 eV due to hydroxide [2]. As shown in Fig. 2, the intensity of V_O peak increases with the increase in Ga content in the films sintered at 300°C, whereas it becomes minimum at Ga contents of 20 and 40 % in the films sintered at 800°C.

The inset in Fig. 3 shows PL spectra observed in IGZO films with Ga contents of 0 and 80 % sintered at 300°C, while Fig. 3 shows the intensities of the PL at 2.5 eV as a function of Ga content. The 2.5-eV PL has a similar Ga-content dependence to the O1s intensity due to oxygen vacancy shown in Fig. 2. A similar PL appearing in ZnO at 2.36 eV has been attributed to oxygen vacancy [3]. Thus, the present 2.5-eV PL should be due to oxygen vacancy. This indicates that PL can detect the presence of oxygen vacancies in IGZO films.

It has also become clear that the on-current becomes maximum when the density of oxygen vacancies is minimized, namely, at Ga content of 0% for the films sintered at 300°C or at 40% for the films sintered at 800°C. These results indicate that oxygen vacancies act as electron scattering centers.

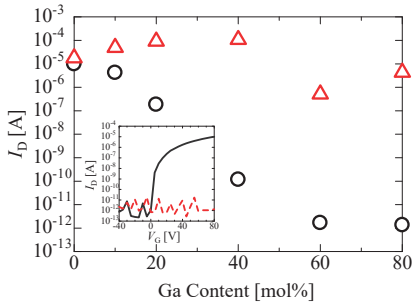

Fig. 1. I_D as a function of Ga content measured at V_G = 80 V for IGZO films sintered at 300 (○) and 800 °C (Δ). (Inset) Transfer characteristics measured at V_D = 40 V for IGZO films with Ga contents of 0 (—) and 80% (---) sintered at 300°C.

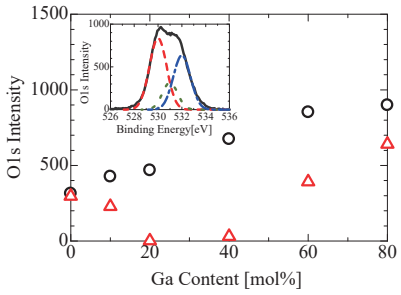

Fig. 2. Intensities of O1s XPS component due to oxygen adjacent to oxygen vacancy (V_O) in IGZO films sintered at 300 (○) and 800 °C (Δ), as a function of Ga content. (Inset) O1s spectrum of IGZO film with Ga content of 0% sintered at 300°C (—) and its components due to oxygen bonding with metal (---), V_O (···), and hydroxide (-•-).

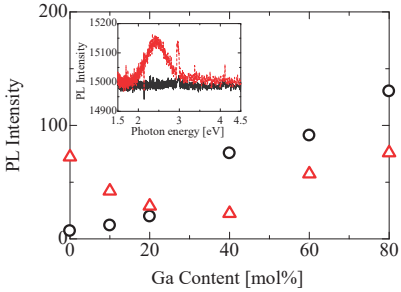

Fig. 3. PL intensities due to oxygen vacancy in IGZO films sintered at 300 (○) and 800 °C (Δ). (Inset) PL spectra of IGZO films with Ga contents of 0 (—) and 80% (---), sintered at 300°C.

[1] S. Ogura *et al.*, Flex. Print. Electron. **1** (2016) 045001.
[2] K. K. Banger *et al.*, Nature Mat. **10** (2011) 45.
[3] K. Vanheusden *et al.*, J. Appl. Phys. **79** (1996) 7983.

BL4U

STXM Analysis of Adsorbent for Effective Recovery of Radioactive Elements

Y. Sano[1], S. Watanabe[1], Y. Miyazaki[1], S. Kibe[1], H. Matsuura[2], T. Uchiyama[2] and Y. Katai[2]
[1]*Japan Atomic Energy Agency (JAEA), Tokai 319-1194, Japan*
[2]*Tokyo City University, Tokyo 158-8557, Japan*

Spent nuclear fuels generated from nuclear power plants contain U and Pu which can be reused, and several long-lived radioactive elements. It will be quite important for effective utilization of energy and environmental loading reduction to process the spent fuel adequately. JAEA has been developing the selective recovery process of radioactive elements, which uses adsorbents of SiO_2 supports coated with styrene-divinylbenzene (SDB) copolymer (SiO_2-P) and extractants on its surface. Scanning transmission X-ray microscopy (STXM) is one of useful techniques to obtain the information about such an adsorbent surface. Our previous study using STXM analysis showed that the SDB polymer and extractants were distributed within several hundred nanometers from the pore surface in SiO_2 supports, and their distributions were spread by the increase of crosslinking degree of polymer (CDP) [1]. In this study, the change of adsorbent surface, such as thickness of polymer and uniformity of extractants, after adsorbing metal ions was investigated by STXM analysis.

The adsorbents in which Di-(2-ethylhexyl) phosphoric acid (HDEHP) was impregnated as an extractant were synthesized by the flowsheet reported by Wei et al. [2]. The average diameter and pore size of the SiO_2 supports were 50 μm and 600 nm, respectively. Some adsorbents were mixed with Zr/HNO_3 solution and filtered for preparing the adsorbents adsorbing Zr. These adsorbents were sliced to 300 nm in thickness by focused ion beam (FIB), and were supplied to STXM analysis.

The O-NEXAFS spectra observed on the adsorbents before and after adsorbing Zr were shown in Fig. 1. The intensity of pre-edge peak at 532 eV increased after Eu adsorption at any position in the adsorbent. Figure 2 shows the colorized composition maps on the cross section of sliced adsorbents before and after adsorbing Zr, which were calculated by fitting C-NEXAFS spectra with those of SDB polymer and HDEHP. The SDB polymer and HDEHP were distributed within several hundred nanometers from the pore surface, and their distributions, especially SDB polymer, were spread uniformly in the adsorbent adsorbing Zr.

The increase of pre-edge peak at 532 eV in O-NEXAFS spectra after Zr adsorption indicates the adsorption of some kinds of molecules contained in Zr/HNO_3 solution, such as H_2O. The adsorption of Zr and these molecules will bring the swelling of SDB polymer in the pore of SiO_2 support, which was observed in Fig. 2. The excessive swelling of SDB polymer is undesirable for the recovery process of radioactive elements. It will be important to select the appropriate pore size in SiO_2 support and coating condition (thickness and CDP) of SDB.

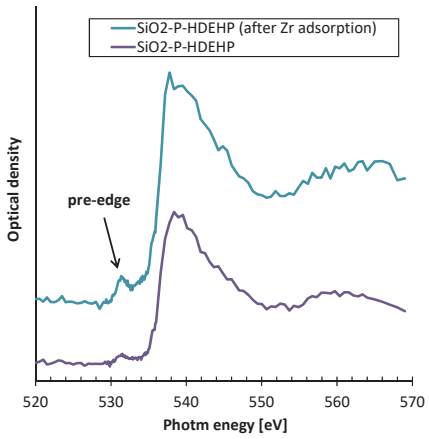

Fig. 1. Change of O-NEXAFS spectra (O-K edge).

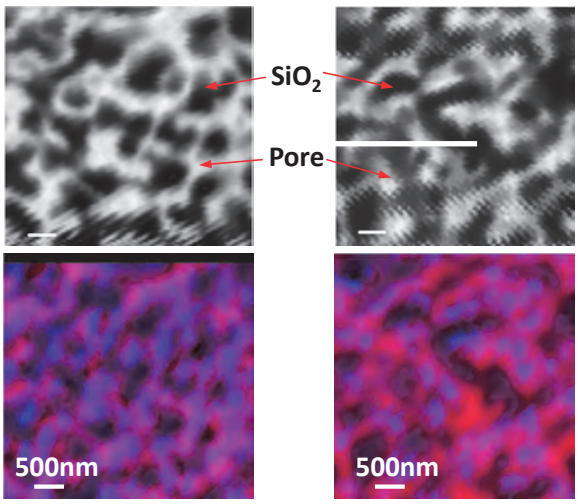

(a) before Zr adsorption (b) after Zr adsorption

Fig. 2. Colorized composition maps (black; SiO_2, white; pore, red; SDB, blue; HDEHP (purple; mixture of red and blue)).

[1] Y. Sano, S. Watanabe and S. Kibe, UVSOR Activity Report **43** (2016) 120.
[2] Y. Wei, M. Kumagai and Y. Takashima, Nucl. Technol. **132** (2000) 413.

BL4B

Nanoscale Magnetic Coupling at the Interface of Mn/Fe Thin Film Heterostructures

T. Miyamachi[1], S. Nakashima[1], Y. Takahashi[1], T. Hattori[1], Y. Takagi[2, 3], M. Uozumi[2, 3], T. Yokoyama[2, 3] and F. Komori[1]

[1]*Institute for Solid State Physics, University of Tokyo, Kashiwa 277-8581, Japan*
[2]*Department of Materials Molecular Science, Institute for Molecular Science, Okazaki 444-8585, Japan*
[3]*Department of Structural Molecular Science, The Graduate University for Advanced Studies (SOKENDAI), Okazaki 444-8585, Japan*

Electronic and magnetic properties of a multilayer system strongly rely on its interfacial conditions. In the case of a magnetic heterostructure composed of antiferromagnetic (AFM) and ferromagnetic (FM) thin films, the strength of the magnetic coupling at the AFM/FM interface, e.g., the exchange energy, is considerably lower for experimental values compared to theoretical ones with the ideal interface. This difference is mainly attributed to the interface roughness caused by intermixing or alloying between AFM and FM layers. Thus, detailed information on the AFM/FM interface structure is essential to understand its intrinsic magnetic coupling. In this study, we performed a complementary study for structural, electronic and magnetic properties of the AFM/FM Mn/Fe thin film heterostructures in combination with scanning tunneling microscopy (STM) and x-ray absorption spectroscopy/x-ray magnetic circular dichroism (XAS/XMCD) [1].

7 monolayer (ML) Fe thin films on Cu(001) in the fcc phase were chosen as a FM layer. AFM Mn layers with a thickness ranging from 0 to 5 ML were subsequently grown at room temperature in ultrahigh vacuum. The electronic and magnetic properties of fcc Fe thin films are sensitive to the structural variation on the surface [2], which is advantageous to investigate the impact of the interface roughness on the magnetic coupling of the AFM/FM thin film heterostructure. The growth and structural properties of the heterostructures were checked by STM before XAS/XMCD measurements.

The XAS/XMCD measurements were performed at BL4B in UVSOR at B = 0, ± 5 T and T = 80 K. The spectra were recorded in the total electron yield mode in the normal (NI :θ = 0°) and the grazing (GI: θ = 55°) and incidences. Note that θ is the angle between the sample normal and the incident x-ray. The XMCD is defined as $\mu_+ - \mu_-$, where μ_+ and μ_- denote XAS at the Fe $L_{2,3}$ adsorption edge with the photon helicity parallel and antiparallel to the sample magnetization.

Figure 1 (a) displays XAS and remanent (± 5 → 0 T) XMCD spectra of bare 7 ML Fe/Cu(001). As previously reported by surface magneto-optic Kerr effect measurements [3], the XMCD signal arising from ferromagnetically-coupled top two Fe layers is slightly larger in NI than GI geometry, indicating the magnetic easy axis towards out-of-plane direction.

In contrast, we find that adding Mn layers induces the spin reorientation transition (SRT) to Fe layers. Figure 1 (b) displays XAS and remanent (± 5 → 0 T) XMCD spectra of 5 ML Mn/ 7ML Fe/Cu(001). The absence of the XMCD signal in GI geometry is observed, while the XMCD signal in NI geometry is nearly unchanged. The result demonstrates the SRT from out-of-plane to in-plane directions. In addition, the enhanced magnetic anisotropy is expected from the larger difference in the XMCD signal between NI and GI geometries. An Mn-thickness dependence of the XMCD signal combined with atomically-resolved STM observations on the surfaces with thin Mn thickness ranges (0-3 ML) reveal that the SRT is driven by the alloy formation in the vicinity of the Mn/Fe interface.

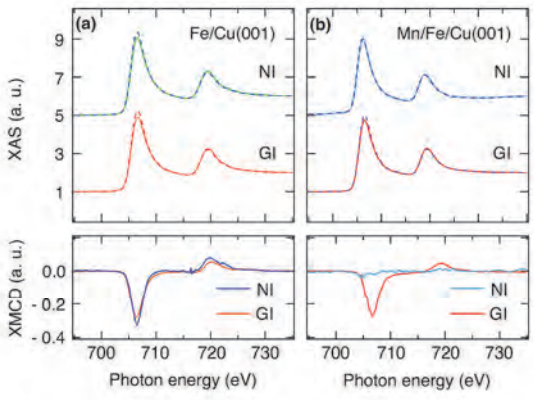

Fig. 1. Fe $L_{2,3}$ edge XAS and remanent XMCD spectra of (a) bare 7 ML Fe/Cu(001) and 5ML Mn/7ML Fe/Cu(001) at NI and GI geometries. Solid and dashed lines for XAS spectra represent μ_+ and μ_-, respectively.

[1] S. Nakashima *et al.*, submitted.
[2] T. Miyamachi *et al.*, Phys. Rev. B **94** (2016) 045439.
[3] J. Thomassen *et al.*, Phys. Rev. Lett. **69** (1992) 3831.

BL4B

XMCD Measurements on a Ferromagnet/Topological Insulator Heterostructure

R. Nakanishi[1], R. Akiyama[1], Y. Okuyama[2], Y. Takagi[3], T. Yokoyama[3], S. Hasegawa[1] and T. Hirahara[2]

[1]*Department of Physics, University of Tokyo, Tokyo 113-0033, Japan*
[2]*Department of Physics, Tokyo Institute of Technology, Tokyo 152-8551, Japan*
[3]*Department of Materials Molecular Science, Institute for Molecular Science, Okazaki 444-8585, Japan*

Topological insulators (TI) are extensively studied recently due to its peculiar properties [1]. The Dirac-cone surface states of TI are protected by time-reversal symmetry (TRS) and backscattering among these surface states is prohibited. But when TRS is broken by application of a magnetic field or incorporating magnetic materials, a gap opening in the Dirac cone is expected and an intriguing phase called the quantum anomalous Hall state can be realized [2]. This phase is expected to show even more exotic phenomena such as the topological magnetoelectic effect. To realize such state, two types of sample fabrication techniques have been employed up to now: (1) magnetic doping while growing the single crystal or thin film of TI [3], and (2) magnetic impurity deposition on the surface of TI [4]. While method (1) was successful and showed evidence of the TRS violation, no one has succeeded using method (2), which should be a more direct way to examine the interaction between the topological surface states and magnetism.

Previously, we have found that when we make a heterostructure of Bi_2Se_3 (TI) and a magnetic insulator $MnBi_2Se_4$, it is possible to observed a massive Dirac cone with a gap of ~ 80 meV. This is a novel method to incorporate magnetism into topological insulators. The calculated band structure reproduced the experimental observation nicely, and the gap opening was reasonably explained as due to the time-reversal symmetry breaking of the Dirac cone due to the ferromagnetic $MnBi_2Se_4$. In the present work, we have performed XMCD measurements at BL4B to experimentally prove that the $MnBi_2Se_4/Bi_2Se_3$ is ferromagnetic. Figure 1 shows the X-ray absorption (XAS) spectra and the corresponding XMCD spectra at 5T. One can find clear XMCD peaks at the Mn L_3 and L_2 edges. The measurements were also performed at remanence, and the result is shown in Fig. 2. Although very weak, one can find a dip structure at the L_3 edge and this shows that the heterostructure is ferromagnetic, consistent with the prediction of the ab initio calculations.

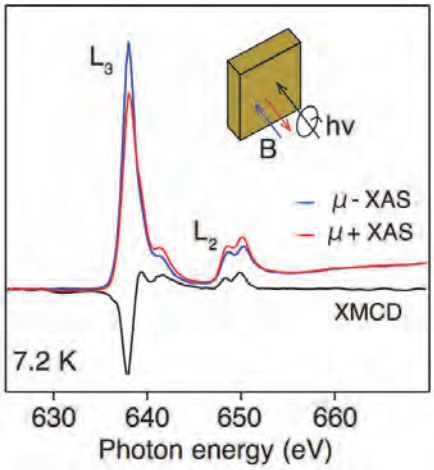

Fig. 1. XAS and XMCD spectra at 5T.

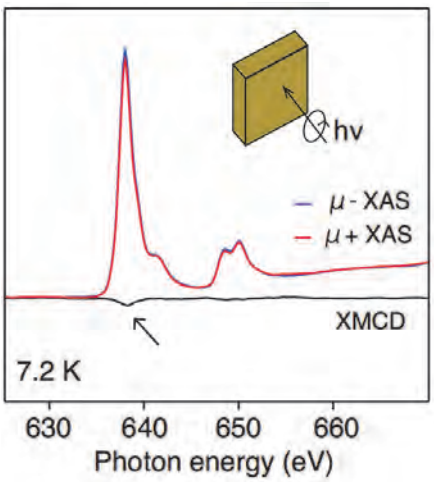

Fig. 2. XAS and XMCD spectra at remanence.

[1] M. Hasan and C. Kane, Rev. Mod. Phys. **82** (2010) 3045.
[2] X.-L. Qi and S.-C. Zhang, Rev. Mod. Phys. **83** (2011) 1057.
[3] For example, C. Z. Chang *et al.,* Science **340** (2013) 167.
[4] For example, M. Ye *et al.,* Phys. Rev. B **85** (2012) 205317.

BL4B

XMCD Study of Ferro Orbital Ordered System: FeV_2O_4

J. Okabayashi[1*] and S. Miyasaka[2]

[1]*Research Center for Spectrochemistry, University of Tokyo, Tokyo 113-0033, Japan*

[2]*Department of Physics, Osaka University, Toyonaka 560-0043, Japan*

The orbital degree of freedom has attracted interest in the condensed-matter physics because of adding of new functional functionalities. Couplings between orbital and spin degrees of freedom in transition metal (TM) oxides exhibit a wide variety of interesting physical phenomena studied in strongly correlated electron systems. The orbital degeneracy of t_{2g} or e_g orbitals, split by the crystal field in TM oxides, gives rise to the orbital ordering phenomena in perovskite-type Fe or V oxides accompanied by Jahn-Teller distortion. Spinel-type FeV_2O_4 is a candidate to study orbital ordering since orbital magnetic moments of Fe^{2+} (d^6) are strongly affected by the Jahn-Teller distortion in the Fe sites, which brings the ferro orbital ordering in V sites through the spin-orbit interaction. An unresolved issue related to orbital ordering of spinel-type vanadium oxides is the relationship between the orbital magnetic moments in vanadium sites and orbital ordering [1]. In case of FeV_2O_4, the V orbital states consist of complex wave functions of degenerated *yz* and *zx* states, which expect the ferro-orbital ordering with the large orbital moments of almost 1 μ_B. On the other hand, in the case of MnV_2O_4, real wave functions in the V sites which are described as d_{yz} and d_{zx} are ordered alternatively, resulting in an antiferro orbital ordering with quenching orbital moments. Therefore, the investigation of orbital moments in V sites enables to discuss the types of orbital ordering. X-ray absorption spectroscopy (XAS) and X-ray magnetic circular dichroism (XMCD) with the sum-rule analysis enables to estimate the orbital moments. In this study, we investigated the element specific electronic and magnetic properties of FeV_2O_4 using XAS and XMCD, and examined the relationship between orbital magnetic moments and orbital ordering.

Single crystals were grown by the floating-zone method. The magnetic and orbital ordering temperatures of FeV_2O_4 were estimated to be 110 K and 70 K, respectively, accompanying the lattice distortions from tetragonal to orthorhombic structures with decreasing temperature. The XAS and XMCD measurements were performed at BL4B, UVSOR, Institute of Molecular Science. Total photoelectron yield mode by directly detecting the sample current was adopted. A magnetic field of ±5 T was applied along the direction of the incident polarized soft x-ray.

Figure 1 shows XAS, XMCD spectra of Fe and V $L_{2,3}$-edge regions taken at 5 K, which is sufficiently lower than the orbital ordered transition temperature. The resulting residuals from the XMCD integrals for both L_2 and L_3 edges suggest that the finite values of orbital magnetic moments remain in the V^{3+} states, which is consistent with the ferro orbital ordering. Using the integrals over XAS spectra and assuming that the V 3*d* electron number to be 2, we deduced the orbital magnetic moments (m_l) to be less than 0.1 μ_B/(V atoms) from the orbital sum rule. This value is small but finite. This result indicates that unquenched orbital magnetic moments contribute to the formation of the complex wave functions in V sites that the d_{yz}+id_{zx} type wave functions consist of the ground states. Although the Fe *L*-edge XAS includes the oxidized states, the finite orbital moments also remain in the Fe sites through the Jahn-Teller distortion.

The t_{2g} states in V 3*d* states are split into two levels by the tetragonal distortion and the lowest *xy* states are occupied by one of the electrons. The other electron occupies the *yz* or *zx* states. The existence of the small but finite orbital magnetic moments in the V sites can be explained by the (i) complex orbital ordering as discussed in the case of FeV_2O_4, (ii) domain formation, and (iii) mixing of the real and complex orbital orderings due to the trigonal distortion around the V sites [2].

We acknowledge to Prof. T. Yokoyama, Dr. Y. Takagi, and Dr. K. Uemura for the technical supports at BL4B.

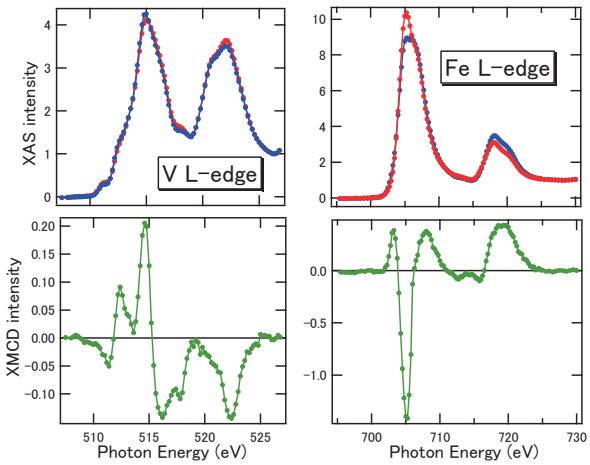

Fig. 1. V and Fe *L*-edge XAS and XMCD spectra in FeV_2O_4.

[1] Y. Nii *et al.*, Phys. Rev. B **86** (2012) 125142.
[2] J. Okabayashi *et al.*, J. Phys. Soc. Jpn. **84** (2015) 104703.

*e-mail: jun@chem.s.u-tokyo.ac.jp

BL4B

Oxygen Adsorption on Single and Double Fe Ultrathin Films

T. Nakagawa[1], T. Nomitsu[1], M. T. Kibria[1], S. Mizuno[1], Y. Takagi[2] and T. Yokoyama[2]
[1] *Department of Molecular and Material Sciences, Kyushu University, Kasuga 816-0955, Japan*
[2] *Institute for Molecular Science, Okazaki 444-8585, Japan*

Iron oxides have been widely studied both due to fundamental research interests and its application for catalysis and solid devices. However, the magnetism of its thinnest unit, a single layer Fe oxide, and the Fe thin films with oxygen adsorption have not been well studied [1]. The magnetic order at the surface of oxide has not been well understood yet [2, 3].

Experiments were done in the x-ray magnetic circular dichroism (XMCD) endstation with the base pressures of 2×10^{-8} Pa for sample preparation and better than 1×10^{-8} Pa for XMCD measurement. Single and double Fe layers were grown on W(110). Oxygen was dosed via a variable leak valve at 2×10^{-7} Pa with the sample kept at the room temperature, and the Fe films exposed up to 150 L(1 L = 1.3×10^{-4} Pa s) of oxygen were examined by XMCD. XMCD spectra were taken with a circularly polarized light (circularly polarization ~ 0.6) at $H = \pm5$ T at a sample temperature of 8 K.

Figure 1 shows x-ray absorption spectra (XAS) and XMCD spectra for single and double Fe layers with increasing the oxygen exposure. At 150 L, XAS for the single layer (SL) and double layer (DL) show splitting at the L_2 edges, which indicates a transition from metallic to oxide states. XMCD signals both for the SL and DL are almost zero. On the contrary, at least up to 5 L, the L_2 edges does not show splitting, which indicates that the Fe films are in metallic states.

On the SL, at 0.2 L, corresponding to ~1/4 monolayer oxygen adsorption, the magnetic moment that is a sum of spin and orbital magnetic moments drastically decreases to 0.4 μ_B, which is much smaller than that of the clean SL, 2.1 μ_B. After 5 L, the magnetic moment is restored to 1.1 μ_B. At 150 L exposure of oxygen, the XMCD single is almost zero.

On the DL, at 0.2 L, XMCD does not change much as compared with that for the clean DL. The magnetic moment at 0.2 L is 2.0 μ_B. With increasing the oxygen exposure, the magnetic moment slowly decreases and it is 1.6 μ_B at 5 L.

With increasing the oxygen adsorption, the SL rapidly loses its ferromagnetic order, resulting in reduced magnetic moments. On the other hand, the DL maintains its magnetic moment until it is oxidized, although the magnetic moment for the DL monotonically and slowly decreases with increasing the oxygen adsorption. This different is attributed to ferromagnetic coupling. On the SD, the oxygen adsorption strongly weakens its ferromagnetic order. However, on the DL, the second layer Fe in the proximity of the W substrate, which is not directly affected by oxygen adsorption, ferromagnetically couples with the topmost Fe layer.

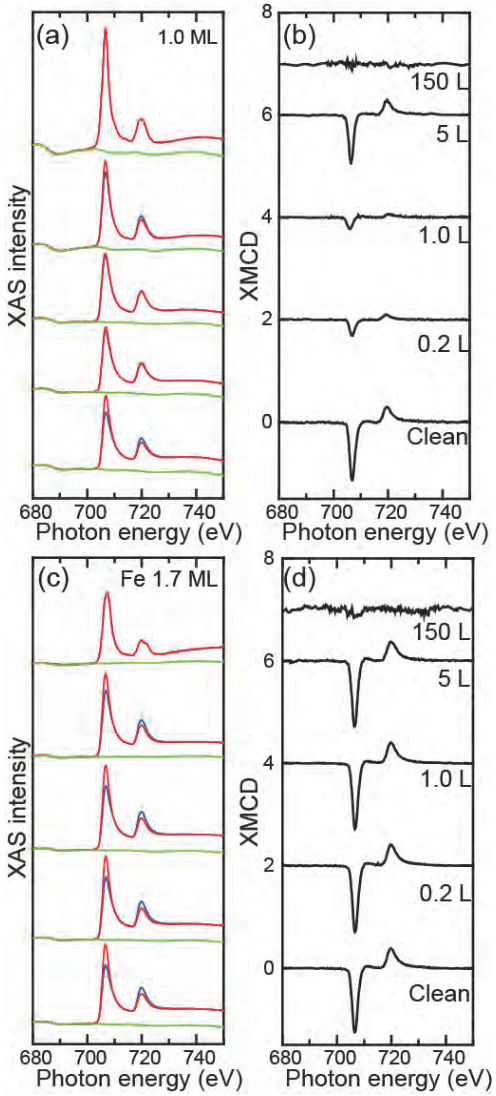

Fig. 1. XAS and XMCD spectra for single (1.0 ML) and double (1.7 ML) Fe layers with increasing oxygen exposure (0 ~ 150 L). (a) XAS spectra taken at ±5 T for the single iron layer (SL). (b) XMCD spectra for SL. (c) the same as (a), but for the double layer (DL). (d) the same as (b), but for DL.

[1] K. Feindl *et al*., Surf. Sci. **617** (2013) 183.
[2] K. Mori *et al*., Phys. Rev. B **72** (2005) 014418.
[3] E. Vescovo, Phys. Rev. B**74** (2006) 026406.

BL4B

XMCD Study of Fe Nanoparticles Synthesized on h-BN Nanomesh

S. Sakai[1, 2], T. Watanabe[1, 2], Y. Yamada[2], S. Entani[1], A. Koide[3], Y. Takagi[3] and T. Yokoyama[3]

[1]*Quantum Beam Science Research Directorate / QST Future laboratory, National Institutes for Quantum and Radiological Science and Technology QST, Tokai 319-1106, Japan*

[2]*Japan Institute of Applied Physics, University of Tsukuba, Tsukuba 305-8577, Japan*

[3]*Department of Materials Molecular Science, Division of Electronic Structure, Institute for Molecular Science, Okazaki 444-8585, Japan*

Tailoring magnetic properties of nanomagnets is the central research issue in developing magnetic and spintronic memory devices. Recent studies have demonstrated graphene-induced perpendicular magnetic anisotropy in a ultra-thin cobalt film on graphene [1, 2] and at the interface region of graphene/Ni(111) [3]. It was also shown that in Co atoms on graphene/metal substrate the magnetization easy axis of the Co atoms changes by the choice of the metal substrate [4]. In addition, single layer graphene and hexagonal boron nitride on Rh(111) and Ru(0001) (so-called graphene and h-BN nanomesh) were shown to be useful as a template for fabricating regularly-arranged nanoparticles of magnetic metals [4-6] relevant to the nanoscale periodicity of the Moiré pattern. The above results in the previous studies make the magnetic metal/atomic layer material structures promising for the magnetic and spintronic memory device applications.

In this study, we investigated the magnetic property of Fe nanoparticles synthesized on h-BN nanomesh (h-BN/ Ru(0001)) with X-ray magnetic dichroism (XMCD) spectroscopy. Total electron yield X-ray absorption (XAS) and XMCD measurements were performed at BL-4B of UVSOR III using an ultra-high-vacuum XMCD apparatus with a base pressure of 10^{-8} Pa. The sample was prepared *in-situ* by depositing Fe on the surface of h-BN/Ru(0001) at ambient temperature. The Fe $L_{2,3}$ edge XAS and XMCD were measured at low temperatures (6.8 K and 140 K) under the magnetic field up to 5 T.

Figure 1 shows the atomic force microscopy (AFM) image of the Fe/h-BN/Ru(0001) sample after the deposition of Fe with a nominal thickness of 1.4 nm. The AFM image and the height cross section profile indicate planar Fe nanoparticles with a mean diameter of ~10 nm and the thickness less than 2 nm.

Figure 2 shows (a) the Fe $L_{2,3}$ edge XAS spectra of the same sample at 6.8 K measured under the grazing incidence (30º) and by applying the magnetic fields of ±5 T (the red and blue lines represent the spectra under the conditions of the circular x-ray vector parallel and antiparallel to the magnetic field) and the magnetic hysteresis loops at 6.8 K and 140 K under the (b) normal and (c) grazing incidence as a function of the magnetic field, which were measured for the L_3 edge absorption intensity. A clear XMCD signal from the Fe nanoparticles was detected as shown in Fig. 2 (a). The Fe nanoparticles are found to be ferromagnetic and have an in-plane easy axis of magnetization as can be judged from the good coincidence between the hysteresis at 6.8 K and 140 K and the change of the curve shape by the incidence direction in Figs. 2 (b) and 2 (c). The magnetic anisotropy field is roughly estimated to be 0.6 T from the intercept of the normal and grazing incidence curve, which is reasonably attributed to the shape anisotropy of the planer Fe nanoparticles (Fig. 1).

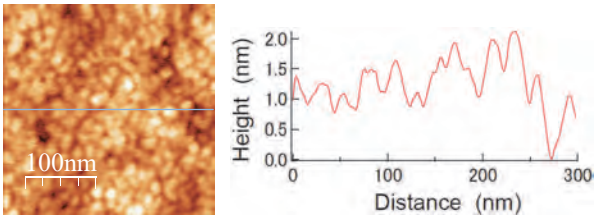

Fig. 1. (left) AFM image and (right) the height cross section profile of 1.4 nm Fe/h-BN/Pt(111)

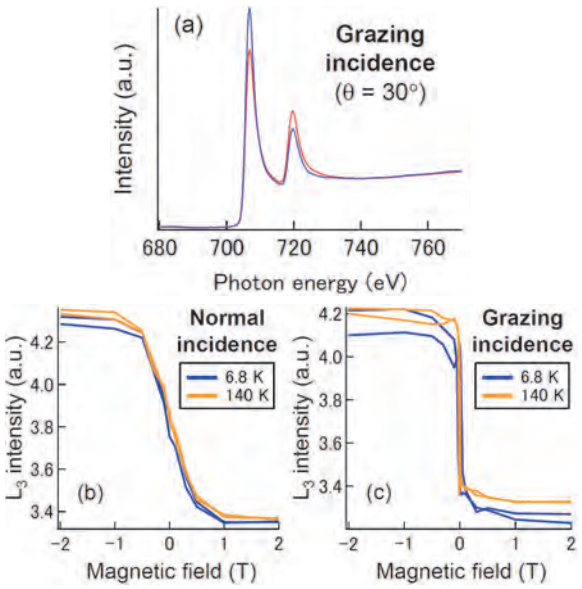

Fig. 2. (a) Fe $L_{2,3}$ edge XAS spectra of 1.4 nm Fe/h-BN/Pr(111) at 6.8 K under the grazing incidence and the hysteresis at 6.8 K and 140 K of the Fe L_3 intensity under the (b) normal and (c) grazing incidence

[1] C. Vo-Van *et al.*, New J. Phys. **12** (2010) 103040.
[2] J. Coraux *et al.*, J. Phys. Chem. Lett. **3** (2012) 2059.
[3] Y. Matsumoto *et al.*, J. Mater. Chem. C **1** (2013) 5533.
[4] F. Donati *et al.*, Phys. Rev. Lett. **113** (2014) 177201.
[5] R. Zhang *et al.*, Phys. Rev. B **78** (2008) 165430.
[6] I. Bihuega *et al.*, Surf. Sci. **602** (2008) L95.
[7] B. Wang *et al.*, J. Phys. Chem. Lett. 2 (2011) 2341.

BL5U

Growth and Electronic Structure of Ultrathin Te Films Grown on Bi_2Te_3

Y. Okuyama[1], Y. Sugiyama[1], S. Ideta[2], K. Tanaka[2] and T. Hirahara[1]
[1]*Department of Physics, Tokyo Institute of Technology, Tokyo 152-8551, Japan*
[2] *UVSOR Facility, Institute for Molecular Science, Okazaki 444-8585, Japan*

Chirality is a geometric property of materials and is mostly discussed in chemistry or biology. A chiral molecule/ion is non-superposable on its mirror image (enantiomers) and individual enantiomers are often called as either “right-” or “left-handed”. Some solid crystals also have chirality such as elements tellurium (Te) and selenium (Se). They are trigonal structures that can be regarded as a hexagonal array of helical chains at ambient pressure. They lack inversion symmetry and possess chirality depending on the rotation direction of the screw axis. Due to this peculiar crystal structure, Te shows intriguing properties such as the circular photon drag effect or the current-induced spin polarization.

It is also well known that the physical properties of Te and Se can be tuned by controlling the lattice constant, which can be achieved by applying pressure. They will eventually undergo a structural transition to the monoclinic or the triclinic phases at very high pressure in the order of ~10 GPa. The electronic structure can also be changed from a semiconductor (the band gap is 0.33eV and 2.0 eV for Te and Se, respectively) to a metal by applying pressure. Recently, based on ab initio calculations, it was predicted that Te undergoes a trivial insulator to a strong topological insulator (metal) transition under shear (hydrostatic or uniaxial) strain in the trigonal phase [1]. Furthermore, it was predicted that the lack of inversion symmetry and spin–orbit interaction leads to the existence of Dirac points or Weyl nodes in the band structure of Te or Se [2]. Such states possess an unconventional spin texture and furthermore, if one can fine-tune the lattice constant by carefully controlling the applied pressure, Te and Se are expected to show the Weyl semimetal phase [3].

In the present work, we have attempted to mimic the lattice constant change by growing a thin Te film on a substrate and utilizing the epitaxy to apply strain. We have adopted Bi_2Te_3 as our substrate since it has been reported as a promising material for Te thin film growth [4]. Figure 1 shows the low-energy diffraction (LEED) pattern of the grown films, and we have found that a six domain Te(10-10) film can be grown on Bi_2Te_3 [5]. We have performed angle-resolved photoemission (ARPES) measurements at BL-5U as shown in Fig. 2. The measurement was performed at 30 K. A Dirac-cone like linear dispersion near the Fermi level was found at the H point of the Brillouin zone. Further work is needed elucidate the entire picture of the band structure.

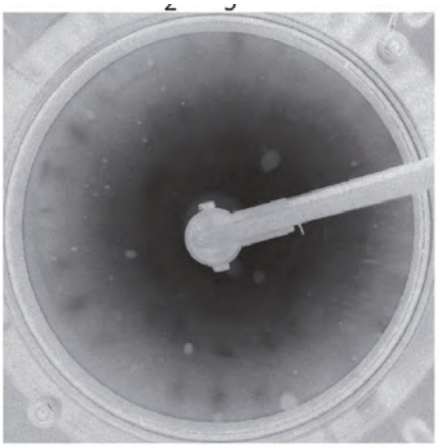

Fig. 1. LEED pattern of the six domain Te(10-10) film grown on Bi_2Te_3.

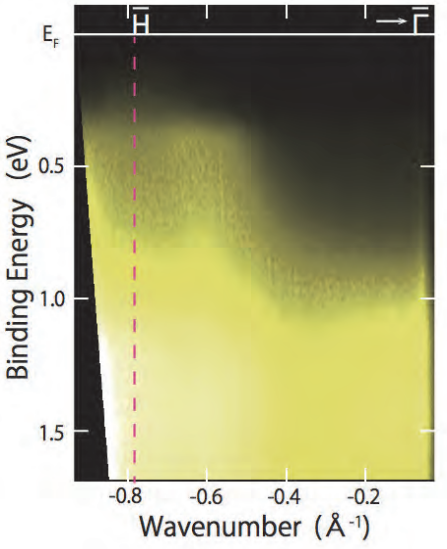

Fig. 2. Band dispersion of the Te(10-10) film near the Fermi level.

[1] L.A. Agapito, N. Kioussis, W.A. Goddard and N.P. Ong, Phys. Rev. Lett. **110** (2013) 176401.
[2] M. Hirayama, R. Okugawa, S. Ishibashi, S. Murakami and T. Miyake, JPS Conf. Proc. **5** (2015) 011024.
[3] M. Hirayama, R. Okugawa, S. Ishibashi, S. Murakami and T. Miyake, Phys. Rev. Lett. **114** (2015) 206401.
[4] K. Hoefer, C. Becker, S. Wirth and L.H. Tjengb, AIP Adv. **5** (2015) 097139.
[5] Y. Okuyama, Y. Sugiyama, S.-I. Ideta, K. Tanaka and T. Hirahara, Appl. Surf. Sci. **398** (2017) 125.

BL5U

Towards Direct Observation of Spatial Modulation on Molecular Orbitals by the Organic–metal Interaction

T. Ueba[1, 2], K. Yonezawa[1], C. Numata[3], R. Shiraishi[2], S. Ideta[1, 2], K. Tanaka[1, 2] and S. Kera[1, 2, 3]

[1]*Department of Photomolecular Science, Institute for Molecular Science, Okazaki 444-8585, Japan*

[2]*School of Physical Sciences, The Graduate University for Advanced Studies (SOKENDAI), Okazaki 444-8585, Japan*

[3]*Department of Nanomaterial Science, Graduate School of Advanced Integration Science, Chiba University, Chiba 263-8522, Japan*

Understanding the weak interaction at the organic-metal interface, including intermolecular interaction and molecule-metal interaction, is of great importance because even such weak interaction can cause the rearrangement of molecular orbitals both in energy and space, which determines the electronic properties at interfaces. Photoelectron angular distribution (PAD) measured by angle-resolved ultraviolet photoelectron spectroscopy (ARUPS) contains information of the spatial distribution and the phase of molecular orbitals (MOs) [1, 2]. Therefore, a careful comparison between experimental and theoretical PADs will enable us to directly discuss a modulation on electronic structures due to the weak interaction. In this work, we performed ARUPS for the perfluoropentacene (PFP, shown in the inset of Figure 1) monolayer film grown on the Ag(111) substrate as a model system, in order to examine how the ARUPS with a photoelectron deflector analyzer in the beam line BL5U shows PAD of MOs.

A PFP monolayer film on Ag(111) was prepared by multilayer deposition on the clean Ag(111) substrate and the following annealing at 400 K, and was kept at 45 ± 5 K during measurements to obtain an ordered structure [3].

Figure 1 (b) shows the k_x-k_y maps converted from ARUPS two-dimensional images measured at $h\nu$ = 60 eV with *p*-polarization, at the respective kinetic energies, as schematically shown in Fig. 1 (a). The momentum k_x is set to be parallel to the Γ-K direction. The energy region I includes merely the *sp*-band of the Ag substrate. In the regions II/III, on the other hand, not only the sharp *sp*-band but also some additional vague structures can be seen. These structures can be attributed to the corresponding MO orbitals, by comparing to the simulated k_x-k_y maps from the PAD simulation [2], as shown Fig. 1 (c).

Unfortunately, even at the lowest photon flux condition (diode current, the pinhole and the exit slit widths were ~350 pA, 4 mm and 100 μm, respectively, at the multi-bunch operation), a radiation damage to the present sample was found, which prevented us to observe clear k_x-k_y maps. For a detailed ARUPS measurement for organic thin films, the photon flux density needs to be further reduced by the use of a defocusing condition or of the single-bunch operation.

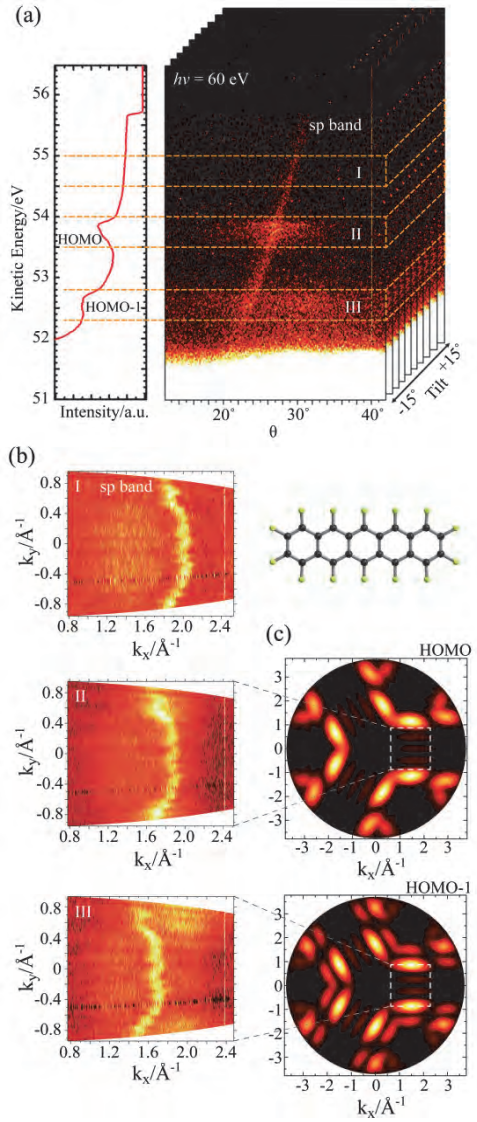

Fig. 1. (a) Angle-resolved UPS image and its angle-integrated spectrum of PFP monolayer on Ag(111). (b) Experimental k_x-k_y maps taken at regions I-III. (c) The corresponding PAD simulation of HOMO/HOMO-1. The three-fold pattern reflects the (111) symmetry. The molecular structure of PFP is also shown in the inset.

[1] P. Puschnig *et al.*, Science **326** (2009) 702.
[2] S. Nagamatsu *et al.*, e-J. Surf. Sci. Nanotechnol. **3** (2005) 461.
[3] M. Marks *et al.*, J, Phys. Chem. C **116** (2012) 1904.

BL5U, BL7U

Two-dimensional Electronic States on InSb(110) Localized in Subsurface Atomic Layers and its Temperature Dependent Energy Shift

Y. Ohtsubo[1, 2], H. Watanabe[1, 2],Y. Yamashita[2], K. Hagiwara[2], S. Ideta[3], K. Tanaka[3] and S. Kimura[1, 2]

[1]*Graduate School of Frontier Biosciences, Osaka University, Suita 565-0871 Japan*
[2]*Department of Physics, Graduate School of Science, Osaka University, Toyonaka 565-0043, Japan*
[3]*UVSOR Facility, Institute for Molecular Science, Okazaki 444-8585, Japan*

On the surface of crystals, two-dimensional (2D) electronic states, so called surface states are formed by two mechanisms as limiting cases [1]. In a localized-bond picture, surface states can be induced by an alternation of the localized chemical bonds due to the reconstruction of the surface atomic structure at the very surface layer. The surface states by such mechanism are usually assumed to have wave functions localized in a few topmost layers. On the other hands, in a perturbed-bulk-band picture, surface states are derived from bulk Bloch states, which are perturbed by the truncation of the periodic potential at the surface and consequently localized at near-surface region. While surface states in general have both characters with varying relative importance, it is sometimes intuitive to consider these two limiting pictures. Recently, there is a renewed interest in the surface states originating from bulk bands, which include the spin-orbital polarized surface states on topological insulators [2] and 2D metallic states on transition-metal oxides [3].

The (110) surface of III-V semiconductors is known to exhibit the well-ordered cleaved surface without any surface reconstruction nor dangling-bond formation [4]. In this project, we observed the surface electronic structure of the InSb(110) cleaved surface. As shown in Fig. 1, two parabolic bands dispersing downwards from the center of surface Brillouin zone was clearly observed by angle-resolved photoelectron spectroscopy (ARPES). Although these band dispersions are quite similar to its bulk-band counterparts, heavy hole and light hole bands, they showed no dispersion along the surface normal checked by changing the incident photon-energy for ARPES. It suggests that these parabolic states have 2D character and derived from the perturbation of the bulk bands by the truncation of the three-dimensional periodicity at the surface. These dispersion of 2D states are similar to the subsurface electronic states on the Ge(111) surfaces covered with various adsorbates [5], suggesting their common origin from subsurface layers of substrates.

Moreover, the 2D states on InSb(110) changed its binding energies depending on the sample temperature. From 13 to 300 K (room temperature), the maximum of the 2D bands moved downwards as large as ~160 meV. Usually, such temperature dependence of semiconductor states are understood due to surface photo-voltage (SPV) effect and surface band bending. However, we have detected a tiny SPV effect by changing the incident photon flux with its sign the opposite to the temperature-driven shift of the 2D bands. Such unusual energy shift can be qualitatively explained by the chemical potential shift due to the low density of states of the conduction bands of InSb [6]. Detailed analysis to understand the temperature-driven energy shifts and further research to use this energy shift to tune energies of the other surface states are in progress.

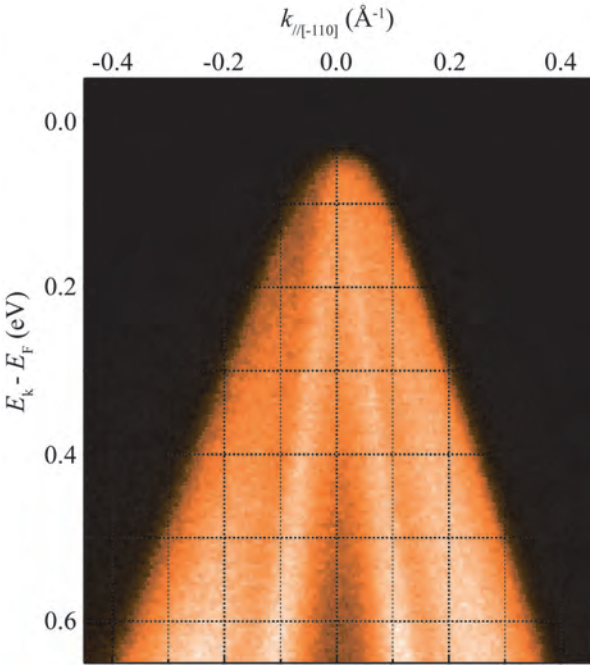

Fig. 1. Surface band dispersion of the InSb(110) cleaved surface observed by ARPES at 13 K ($h\nu$ = 20 eV).

[1] H. Ibarh, *Physics of Surfaces and Interfaces* (Springer-Verlag, Berlin, Heidelberg, 2006).
[2] M. Z. Hasan and C. L. Kane, Rev. Mod. Phys. **82** (2010) 3045.
[3] A. F. Santander-Syro *et al.*, Nature **469** (2011) 189. and K. Yoshimatsu *et al.*, Science **333** (2011) 319.
[4] L. Pfeiffer *et al.*, Appl. Phys. Lett. **56** (1990) 1697.
[5] Y. Ohtsubo *et al.*, Phys. Rev. B **88** (2013) 245310.
[6] L. Walczak *et al.*, Surf. Sci. **608** (2013) 22.

BL5U, BL7U

Surface Electronic Structure of Kondo Insulator SmB_6(111)

Y. Ohtsubo[1, 2], K. Hagiwara[2], C. Wang[2], S. Ideta[3], K. Tanaka[3], F. Iga[4] and S. Kimura[1, 2]
[1]*Graduate School of Frontier Biosciences, Osaka University, Suita 565-0871 Japan*
[2]*Department of Physics, Graduate School of Science, Osaka University, Toyonaka 565-0043, Japan*
[3]*UVSOR Facility, Institute for Molecular Science, Okazaki 444-8585, Japan*
[4]*Department of Physics, Ibaraki University, Mito 310-0056, Japan*

Topological Kondo insulator (TKI) is a new group of topological materials. On the surface of TKI, robust topological surface state (TSS) disperses across a tiny energy gap owing to the strong correlation between itinerant and localized electrons (Kondo effect) [1]. Therefore, TKI phase is realized thanks to the synergetic effect between strong electron correlation and spin-orbit interaction (SOI), which results in the non-trivial parity eigenvalues across the Kondo gap. Since such synergetic effect can cause new exotic physical phenomena, such as superconductivity without inversion symmetry [2], the surface electronic structure of TKI is gathering much attention in these days.

So far, most of the experimental and theoretical studies about TKI have been performed on the (001) cleaved surface of SmB_6 and the surface state exhibits metallic dispersion and spin-polarization, which are the major characteristics of TSS [3-5]. Recently, we found a new TKI, YbB_{12} [6]. On the (001) clean surface of YbB_{12}, angle-resolved photoelectron spectroscopy (ARPES) showed a metallic surface state dispersing across the bulk Kondo gap and its orbital angular momentum (OAM) polarization that is often connected to spin polarization via SOI. For this study, we have established a method to obtain the clean surface of a group of Kondo insulators such as SmB_6 and YbB_{12} in situ without cleaving [7]. The clean surface preparation without cleaving also pave the way to observe the surface electronic states and its topology not only in cleavage planes but in general surfaces of the crystal. It is important to discuss the topological nature of the crystal from its surface states, because the topological order of the bulk crystal should govern the general character of the surface states without regarding detailed atomic structure and mirror indices of the surface plane.

In this project, we studied the electronic structure of the SmB_6(111) clean surface by ARPES. The clean surface of SmB_6(111) cannot be obtained by cleaving but was obtained *in-situ* by heating the single crystal up to 1600 K in an ultra-high vacuum chamber. The quality of the clean surface was evaluated by the sharp and low-background electron diffraction patterns as well as sharp photoelectron spectra itself.

Figure 1 shows the ARPES result indicating the highly dispersive itinerant states which exhibits clear hybridization with nearly localized 4f states lying just below the Fermi level. The hybridized state disperses across the Kondo gap and clearly indicates the metallic dispersion across the Fermi level at the same time. It strongly suggests its topological origin since the similar surface states are expected to appear on different surfaces of the same TKI crystal. Further analysis to understand the topological origin and whole picture of the topological electronic states of SmB_6 is in progress.

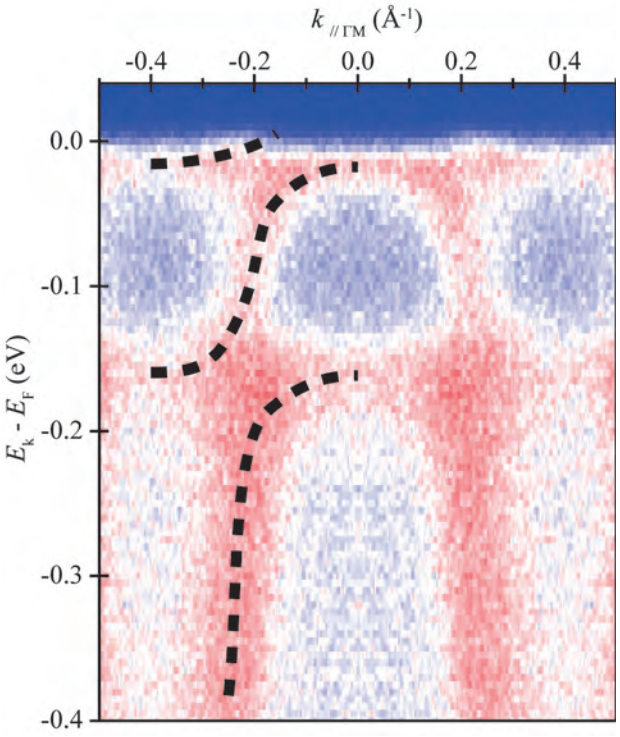

Fig. 1. Surface band dispersion of the SmB_6(111) clean surface observed by ARPES at 13 K ($h\nu$ = 26 eV). Dashed lines are guides to the eye. The ARPES intensities are symmetrized with respect to k = 0 Å^{-1}.

[1] M. Dzero *et al.*, Phys. Rev. Lett. **104** (2010) 106408.
[2] E. Bauer *et al.*, Phys. Rev. Lett. **92** (2004) 027003.
[3] N. Xu *et al.*, Phys. Rev. B **88** (2013) 121102(R).
[4] M. Neupane *et al.*, Nature Commun. **4** (2013) 2991.
[5] J. Jiang *et al.*, Nature Commun. **4** (2013) 3010.
[6] K. Hagiwara, Y. Ohtsubo *et al.*, Nature Commun. **7** (2016) 12690.
[7] K. Hagiwara, Y. Ohtsubo *et al.*, Proc. SCES 2016.

BL5U

Electronic Structure of a (1×1) VO Film on Ag(100): Soft X-ray Photoelectron Spectroscopy Study

Y. Sugizaki[1], H. Motoyama[1] and K. Edamoto[1, 2]
[1]*Department of Chemistry, Rikkyo University, Tokyo 171-8501, Japan*
[2]*Research Center for Smart Molecules, Rikkyo University, Tokyo 171-8501, Japan*

The mechanism of metal-insulator transitions (MITs) in vanadium oxides has been a matter of ongoing controversy for decades. The discussion has been focused on whether the transition is triggered by an electron-lattice interaction (Peierls-type model) or by an electron-electron interaction (Mott-type model), and a vast amount of studies have been performed on the electronic structures of vanadium oxides (mostly VO_2 and V_2O_3). However, very limited information is available on the electronic structure of vanadium monoxide (VO) at present, and it is not clear whether MIT also occurs in VO or not. This is primarily because it is hard to synthesize a VO single-crystal in an atmospheric condition, which makes it difficult to make an experimental study on the electronic structure of VO. Recently we found that a VO(100) single-crystal film can be formed on Ag(100) by reactive deposition of V atoms [1], which would enable the detailed spectroscopic studies on the electronic structure of this substance. In this study, we performed a high-resolution PES study for the VO(100) film on Ag(100).

Experiments were performed at BL-5U of the UVSOR Facility, Institute for Molecular Science. The spectra presented below were measured at the photon energy of 54 eV. In this study, the estimation of the Fermi edge is primarily important, and it was estimated by fitting the spectrum of a gold film attached to the sample holder in the Fermi edge region using Gaussian convoluted Fermi distribution function. The VO(100) film was prepared by electron beam deposition of V atoms in O_2 at 3.0×10^{-7} Pa and subsequent annealing at 450°C for 30 min.

Figure 1. shows the valence band PES spectrum of the VO film on Ag(100) measured at room temperature (red line) and that at 4.86 K (blue line). The band observed at 0 - 4 eV is ascribed to a V 3*d* band, and the band at 4 – 10 eV is ascribed to a V 3*d* – O 2*p* hybrid band (valence band) overlapping with a 4*d* band of the underlying Ag substrate. We measured magnified spectra in the vicinity of the Fermi level (E_F) at both temperatures, and confirmed that there is a clear cut-off in both spectra. The positions of the cut-off were carefully determined by fitting the spectra using Gaussian convoluted Fermi distribution functions, and it was confirmed that the cut-off positions were identical to that observed in the spectrum of the gold film. These results imply that VO in the ground state should have a metallic electronic structure. It has been controversial whether the ground state of VO is a metal or an insulator; for example, Yamazaki et al. made a theoretical study using the energy band calculations utilizing GW approximation and predicted that VO has a metallic nature [2], while Mackrodt et al. proposed that VO in the ground state is a Mott-Hubbard type insulator using a hybrid DFT calculations [3]. We think that the long-standing controversy is settled by the result of the present PES study. In addition, it is found that VO has a metallic nature in the temperature range of 4,86 K – room temperature. This result suggests that MIT does not occur in VO unlikely to the case of other vanadium oxides.

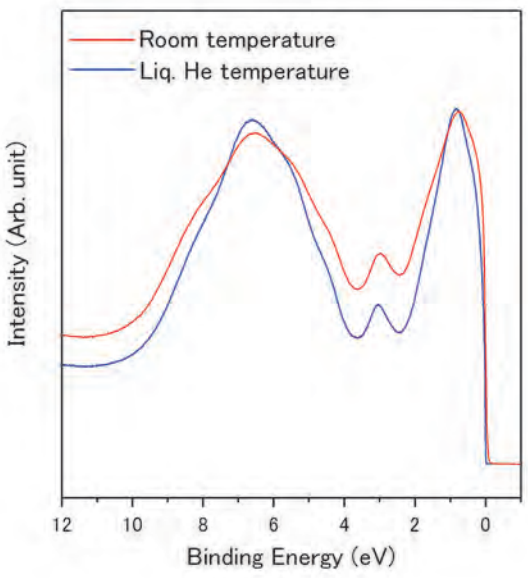

Fig. 1. The PES spectrum of the VO(100) film on Ag(100) measured at room temperature (red line) and that at 4.86 K (blue line) (*hv* = 54 eV).

[1] T. Nakamura *et al.*, Jpn. J. Appl. Phys. **55** (2016) 075501.
[2] A. Yamasaki and T. Fujiwara, Phys. Rev. B. **66** (2002) 245108.
[3] W. C. Markrodt *et al.*, Phys. Rev. B. **69** (2004) 115119.

BL5B

Vacuum Ultra-Violet Absorption Spectra of Amorphous Chalcogenide Semiconductor Thin Films

K. Hayashi

Department of Electrical, Electronic and Computer Engineering, Gifu University, Gifu 501-1193, Japan

Amorphous chalcogenide semiconductor materials, such as a-As_2S_3, a-As_2Se_3 and a-Se etc., show a variety of photo-induced phenomena. Therefore, these materials are expected as materials for optoelectronic devices. A lot of work have been done on the photo-induced phenomena of these amorphous semiconductor materials and various mechanisms have been proposed for these photo-induced phenomena [1-3]. However, the details of the mechanisms are still unknown. For device applications, it is necessary to sufficiently understand the fundamental properties of these materials. These phenomena were studied by exciting outer core electrons with the irradiation of light with the energy corresponding to the optical bandgap or sub-bandgap. The interest has been attracted for the change of the optical properties in the energy region of the visible light. We are interesting for the changes of the optical properties in the higher energy region. To our knowledge, little attention has been given to photo-induced changes at the vacuum ultra-violet (VUV) absorption spectrum. In this report, we measure the VUV absorption spectra on as-deposited evaporated amorphous As_xSe_{1-x} (for x=0.3, 0.4 and 0.5) thin films.

Samples used for the measurement of the VUV absorption spectra were amorphous As_xSe_{1-x} (for x=0.3, 0.4 and 0.5) thin films prepared onto aluminum thin films by conventional evaporation technique. Using different bulk glass of the composition as a source material, different amorphous film of the compositions was prepared. Typical thickness of the amorphous film and the aluminum film were around 200 nm and 100 nm, respectively. The aluminum film of the thickness of 200 nm was also used in order to eliminate the higher order light from the monochromator in the VUV region. The measurements were carried out at room temperature at the BL5B beam line of the UVSOR facility of the Institute for Molecular Science. And the spectrum was measured by using the silicon photodiode as a detector. Two pinholes of 1.5 mm in a diameter were inserted between the monochromator and sample to remove stray light. The intensity of the VUV light was monitored by measuring the total photoelectron yeild of a gold mesh. The positions of the core levels for the samples were calibrated by referencing to the 2*p* core level absorption peak of the aluminum film.

Figure 1 shows the VUV absorption spectra of as-deposited amorphous As_xSe_{1-x} (for x=0.3, 0.4 and 0.5) thin films in the energy region from 40 to 60 eV. Two main absorption peaks were observed in this energy region. One absorption peak around 44 eV corresponds to the 3*d* core level of arsenic atom. Another absorption peak around 56 eV corresponds to the 3*d* core level of selenium atom. The broad structures observed in the absorption spectra consist of two or more components. The origin of each component is not clear now. I would like to clarify the origin of each component in the future. As shown in figure, the ratio of the two main absorption peaks changes depending on composition of the film. The spectrum shape also changes depending on composition of the film. We think that those changes are related to the local structures of the amorphous network. We will observe the composition dependence of the change in the spectrum before and after irradiation of light in future. And we are going to investigate the relations between those changes.

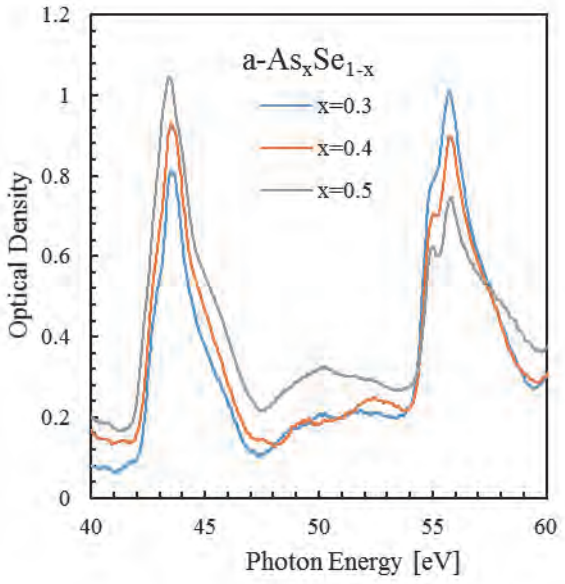

Fig. 1. VUV absorption spectra of as-deposited amorphous As_xSe_{1-x} (for x=0.3, 0.4 and 0.5) thin films in the energy region from 40 to 60 eV.

[1] K. Tanaka, Rev. Solid State Sci. **4** (1990) 641.
[2] K. Shimakawa, A. Kolobov and S. R. Elliott, Adv. Phys. **44** (1995) 475.
[3] K. Tanaka, Encyclopedia of Nanoscience and Nanotechnology **7** (2004) 629.

BL6U

Electronic Structures of Two-dimensional Alloys of Silicon and Germanium

A. Fleurence[1], C. Huet[1], S. Wallace[1], F. Wiggers[3], H. Yamane[2], N. Kosugi[2] and Y. Yamada-Takamura[1]

[1]*School of Materials Science, Japan Advanced Institute of Science and Technology, Nomi 923-1292, Japan*
[2]*Institute for Molecular Science, Okazaki 444-8585, Japan*
[3]*MESA+ Institute for Nanotechnology, University of Twente, 7500 AE Enschede, The Netherlands*

Silicene and germanene are honeycomb lattices made of Si and Ge atoms, respectively, with buckled structures due to the mixed sp^2/sp^3 hybridization in their chemical bondings [1]. The electronic structures calculated for free-standing silicene and germanene both exhibit Dirac cone regardless of the buckling [1].

Although silicon-germanium alloys with diamond structure are known as isomorphous system, up to now, there is no experimental study for their two-dimensional (2D) counterparts.

Silicene and germanene exist only in epitaxial forms. Among them, epitaxial silicene on ZrB_2 thin films grown on Si(111) has the particularity to form in a spontaneous and self-terminating way by segregation of Si atoms from the silicon substrate [2]. Epitaxial silicene forms a ZrB_2(0001)-(2×2) reconstruction and is semiconducting as a 350 meV-wide gap is opened in the Dirac cones.

We had demonstrated by means of low energy electron diffraction (LEED) and scanning tunneling microscopy at our home laboratory that the deposition of germanium on silicene can give rise to silicene-germanene heterostructures, 2D silicene-Ge alloy in the form of Ge incorporation into the silicene lattice, and vertical silicene-germanene heterostack structures, depending on the preparation conditions [3]. The experiments carried out at UVSOR were aimed at getting insights into (i) how Ge atoms are integrated in the silicene lattice and heterostacks, and (ii) what their electronic band structures are.

Water-cooled mini K-cell, which we use for the experiments in our home-based setup, was installed in the preparation chamber of BL6U for evaporating Ge. Epitaxial silicene samples were prepared on-site by annealing ZrB_2/Si(111) samples at 800ºC under ultrahigh vacuum [2]. Ge deposition was realized with a substrate temperature of 350°C.

For low Ge coverages giving rise to silicene-Ge alloy, no significant change in the Si2*p* core-level spectrum are observed and the structure remains ZrB_2(0001)-(2×2)-reconstructed. The Ge core-level (Fig1.(a)) shows a single component which indicates that the Ge atoms are incorporated in a unique site in the silicene lattice. Angle-resolved photoemission spectroscopy (ARPES) spectra (Fig. 1 (b)) indicate that the band structure is essentially the same as that of pristine silicene. In contrast, for coverage beyond 0.2 ML Ge, a complex LEED pattern and a different core-level spectrum (Fig. 1 (c)) suggests a more drastic transformation of the silicene structure related to the growth of a Si-Ge heterostack.

This work was supported by the Joint Studies Program (No. 203, 2016-2017) of the Institute for Molecular Science.

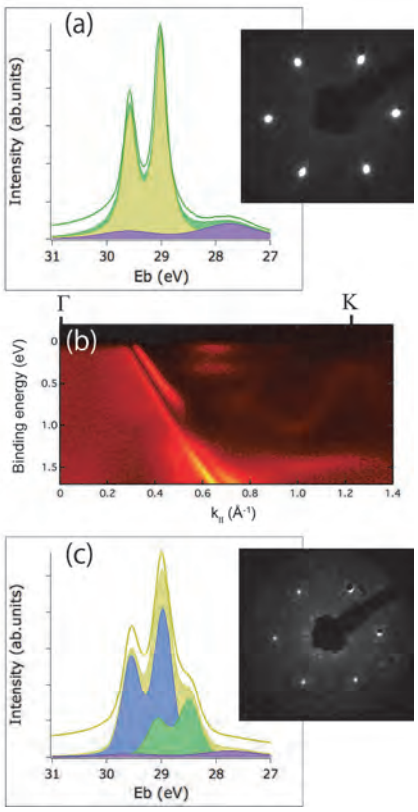

Fig. 1. (a): Ge 3*d* core-level ($h\nu$ = 80 eV) and ZrB_2(0001)-(2×2) LEED pattern (E_B = 40 eV) after deposition of 0.06 ML Ge. (b): ARPES spectra after deposition of 0.04 ML Ge ($h\nu$ = 43 eV). (c): Ge 3*d* core-level ($h\nu$ = 80 eV) and LEED pattern (E_B = 40 eV) after deposition of 0.41 ML Ge. All the measurements were carried out at room temperature.

[1] K. Takeda and K. Shiraishi, Phys. Rev. B **50** (1994) 14916.
[2] A. Fleurence *et al.*, Phys. Rev. Lett. **108** (2012) 245501.
[3] Y. Awatani, A. Fleurence and Y. Yamada-Takamura, Bulletin of the American Physical Society, 2016 March Meeting, T1.307.

BL6U

Bilayer Silicon on ZrB_2(0001)

A. Fleurence[1], F. Wiggers[2], S. Wallace[1], C. Huet[1], H. Yamane[2], N. Kosugi[2] and Y. Yamada-Takamura[1]

[1]*School of Materials Science, Japan Advanced Institute of Science and Technology, Nomi 923-1292, Japan*
[2]*MESA+ Institute for Nanotechnology, University of Twente, 7500 AE Enschede, The Netherlands*
[3]*Institute for Molecular Science, Okazaki 444-8585, Japan*

The experimental observation of silicene provides an evidence that silicon can crystallize in a graphitic form with chemical and physical properties different from those of bulk silicon in which Si atoms are sp^3 hybridized. Even though the graphene-like character of silicene was verified by the observation of π-electronic states [1], the hybridization of the Si atoms in silicene is not pure sp^2 as for C atoms in graphene, but adopts an intermediate sp^2/sp^3 hybridization reflected by the buckling of the honeycomb structure of free-standing silicene [2]. The resulting flexibility of silicene structure makes it less robust than graphene against its environment. Therefore, the possibility of stacking silicene layers in a manner similar to other layered materials such as graphite or chalcogenides is questionable.

It was recently claimed that multilayer silicene can be grown. In our group, we demonstrated that a bilayer silicon can be fabricated on ZrB_2(0001) thin films grown on Si(111) substrates by depositing silicon on the epitaxial silicene sheet that forms spontaneously on the ZrB_2(0001) surface [3]. The resulting bilayer silicon sheet has structural and electronic properties distinct from both silicene and bulk silicon: The bilayer silicon is metallic as the density of states at Fermi level is non zero [3] as shown by tunneling spectroscopy and preliminary characterizations of the band structure by angle-resolved photoemission spectroscopy (ARPES). Low-energy electron diffraction (LEED) pattern shows that the bilayer has a lattice parameter slightly larger than that of silicene. As a consequence, the ($\sqrt{3}\times\sqrt{3}$) unit cell of the bilayer does not commensurate with the (2×2) unit cell of ZrB_2(0001) as that of silicene does.

The purpose of this study was to get a comprehensive picture of the band structure of the Si bilayer by measuring high resolution ARPES spectra along both the Γ-K and Γ-M directions of the Brillouin zone of ZrB_2(0001).

Epitaxial silicene samples were prepared on-site by annealing ZrB_2/Si(111) samples at 800°C under ultrahigh vacuum [1]. Silicon was evaporated by heating a piece of silicon in front of the sample held at a temperature of 320°C. The formation of the bilayer is verified by the observation of features specific to the bilayer silicon in LEED pattern [3]. ARPES spectra were then recorded with a photon energy of $h\nu$=43 eV at a temperature of 20 K.

The parabolic band centered on the M point (which also corresponds to the K point of epitaxial silicene) is reminiscent of the π band observed for epitaxial silicene on ZrB_2(0001).

However, it is shifted upward by 200 meV. In addition, the band structure features several new bands crossing linearly at the Fermi level. The most intense band of these new bands intersect the Fermi level at a position slightly inward with respect to the M point of the Brillouin zone of ZrB_2(0001). This shift is consistent with a silicon structure with a lattice parameter slightly larger than that of epitaxial silicene as previously deduced from LEED patterns [3]. The mismatch between the ZrB_2(0001) unit cell and that of the bilayer silicon causes a back-folding of the linear bands which are replicated near the Γ and M points of the Brillouin zone.

These results may suggest that the silicon layers have slightly different lattice parameters that results in the decoupling of the topmost layer. This hypothesis will be investigated further by *ab-initio* calculations using the conclusions drawn from the experimental data as inputs.

This work was supported by the Joint Studies Program (No. 203, 2016-2017) of the Institute for Molecular Science.

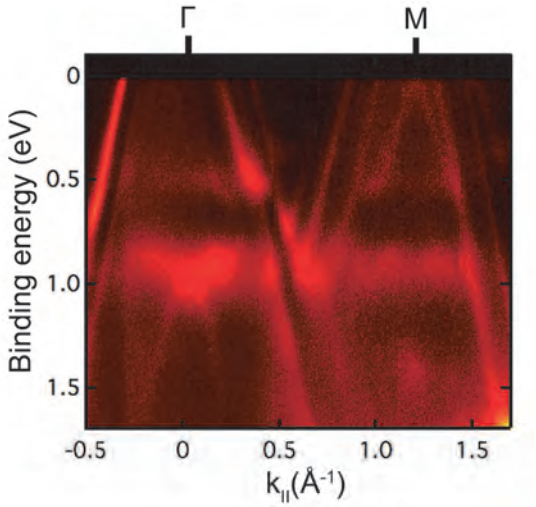

Fig. 1. ARPES spectra of the bilayer silicon along the Γ-M direction of the Brillouin zone of the ZrB_2(0001) recorded with $h\nu$ = 43 eV at 20K.

[1] A. Fleurence *et al.*, Phys. Rev. Lett. **108** (2012) 245501.
[2] S. Cahangirov *et al.*, Phys. Rev. Lett. **102** (2009) 236804.
[3] T. G. Gill *et al.*, 2D Mater. **4** (2017) 021015.

BL6U

Hydrogenation of Epitaxial Silicene on ZrB_2(0001)

A. Fleurence[1], T. Yonezawa[1], S. Wallace[1], S. Horibe[1], T. Kato[1], H. Yamane[2], N. Kosugi[2] and Y. Yamada-Takamura[1]

[1]*Japan Advanced Institute of Science and Technology, Nomi 923-1292, Japan*
[2]*Institute for Molecular Science, Okazaki 444-8585, Japan*

Silicene is a 2D Dirac material made of a Si honeycomb lattice [1]. However, in contrast to its analogue, graphene, for which the sp^2 hybridization of the orbitals makes the structure perfectly planar, the structure of silicene is buckled due to sp^2/sp^3 hybridization [1]. For this reason, it was predicted by theoretical calculations that the hydrogenation of silicene would have an even stronger effect on the structure of silicene than on that of graphene with the opening of a gap as wide as 1.2 eV [2].

ZrB_2 thin films grown on Si(111) has the particularity to promote the spontaneous formation of silicene by segregation of Si atoms from the substrate [3]. This epitaxial form of silicene has a structure in which all atoms but one are laying at the same height and one is protruding. The band structure is also affected as the Dirac cones are turned into parabolic bands [3].

Previous experiments confirmed that the hydrogenation of epitaxial silicene sheets on Ag(111) [4] and ZrB_2(0001) causes structural change of the silicene structures. In the latter case, this is reflected by a different electron energy dependence of the low-energy electron diffraction (LEED) pattern. The surface is ZrB_2(0001)-(2×2)-reconstructed as pristine silicene does, but for an electron energy (E_B) of 30 eV, the inner fractional spots are not visible anymore.

The purpose of the experiments carried out at BL6U was to get insights into the nature of the change induced by hydrogenation in the structure and the band structure of epitaxial silicene, which has not been reported yet. Si2*p* core-level spectra were recorded at different photon energies including a surface-sensitive photon energy of $h\nu$ = 130 eV. For Angle-resolved photoemission spectroscopy (ARPES), a photon energy of $h\nu$ = 43 eV were used.

Epitaxial silicene samples were prepared on-site by annealing ZrB_2/Si(111) samples at 800ºC under ultrahigh vacuum [3]. Silicene was hydrogenated at room temperature by means of a hot W filament used to crack H_2 molecules fed in the chamber through a leak valve. The complete hydrogenation of silicene was verified by the vanishing of the ZrB_2(0001)-(2×2) fractional spots in LEED pattern recorded with E_B = 30 eV. Fig. 1. (a) compares the Si2*p* core-level spectra recorded before and after hydrogenation of epitaxial silicene. It shows that hydrogenation causes a 0.2 eV shift of the Si2*p* core-level towards higher binding energies. The spectrum features two components broader than those of silicene. More surprisingly, the ARPES spectra shown in Figs. 1. (d) and (e) recorded around the K point of silicene show that all the silicene-related bands (visible between the Fermi level and E_B=1.5 eV) have faded upon hydrogenation whereas those of the ZrB_2 remained.

These results although insightful, suggest that further characterizations by scanning tunnel microscopy are required to determine whether the silicon structure remains two-dimensional upon hydrogenation.

This work was supported by the Joint Studies Program (No. 203, 2016-2017) of the Institute for Molecular Science.

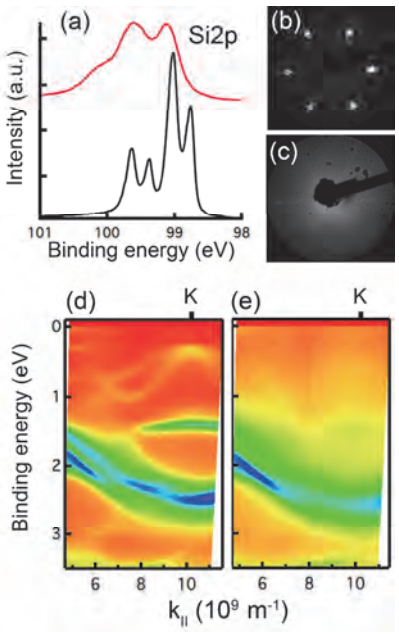

Fig. 1. (a) Si2*p* core-level spectra before (black) and after (red) hydrogenation. (b) and (c): LEED patterns corresponding respectively to the spectra. (d) and (e): ARPES spectra before and after hydrogenation around the K point of silicene. All the measurements were carried out at a temperature of 20K.

[1] K. Takeda and K. Shiraishi, Phys. Rev. B **50** (1994) 14916.
[2] M. Houssa *et al.*, Appl. Phys. Lett. **97** (2010) 112106.
[3] A. Fleurence *et al.*, Phys. Rev. Lett. **108** (2012) 245501.
[4] J. Qiu *et al.*, Phys. Rev. Lett. **114** (2015) 126101.

BL6U

Electronic Structure of GaSe Thin Films Grown on Ge(111) Wafers

T. Yonezawa[1], A. Fleurence[1], H. Yamane[2], S. Wallace[1], S. Horibe[1], T. Kato[1], N. Kosugi[2] and Y. Yamada-Takamura[1]

[1]*Japan Advanced Institute of Science and Technology, Nomi 923-1292, Japan*
[2]*Institute for Molecular Science, Okazaki 444-8585, Japan*

Gallium selenide (GaSe) belongs to a class of material called "metal chalcogenides" which is attracting a lot of interests as a two-dimensional semiconducting material, since a single layer of molybdenum disulfide (MoS_2) was made into a transistor [1]. Like graphite, layers of chalcogenides stack via weak van der Waals interaction, and these layers can be exfoliated easily using adhesive tapes, which is advantageous to prepare atomically-flat and clean surfaces. We are particularly interested in GaSe as a lattice-matching and less-interacting substrate for "silicene" which is a Si-version graphene [2], so that the combination will realize epitaxial silicene with the properties of those of free-standing one.

GaSe thin films used in this study were grown on Ge substrates by molecular beam epitaxy (MBE) method. Ge(111) wafers (undoped) were cleaned ultrasonically with acetone, ethanol, and deionized water. The substrates were then fixed to a molybdenum block with indium, and introduced into the MBE system via a load-lock. Surface oxides were removed by heating the substrates at 600°C under ultrahigh vacuum (UHV). Oxide-free surface kept at growth temperature of 525°C was first exposed to Se vapor for 30 seconds, and then GaSe growth was started by exposing the surface simultaneously to Ga vapor and Se vapor with a flux ratio of Ga/Se = 7/100 for 20 minutes. GaSe growth was monitored *in situ* by reflection high energy electron diffraction, and an epitaxial relationship of GaSe(0001)//Ge(111) and GaSe[11-20]//Ge[1-10] was determined.

For the GaSe thin film surface prepared by cleavage using adhesive tape at UVSOR prior to the introduction to the preparation chamber of BL6U via load-lock, we found traces of carbon in photoelectron spectroscopy results, which are not shown here. Seeing this result, the following measurements were carried out without this preparation process.

Angle-resolved photoemission spectroscopy (ARPES) was carried out on an as-grown GaSe thin film surface using a photon energy of 50 eV at room temperature. GaSe thin film sample was degassed at 300°C under UHV before the measurement. The results are plotted along the Γ-K direction of GaSe(0001), which is shown in Fig. 1. Clear double parabolic bands similar to what has been observed for cleaved GaSe single crystal [3] can be identified, but at larger binding energy indicating possible doping. The lack of feature at K point makes this surface an ideal substrate for free-standing-like silicene.

Raising annealing temperature to 500°C resulted in a change in the low energy electron diffraction (LEED) pattern. As shown in Fig. 2, additional spots appeared around original GaSe(0001)-(1x1) spots which corresponds well with Moiré constructed by GaSe(0001) and Ge(111). This change was associated with loss of oxygen from the surface and change in Ga- and Ge-related states observed by core-level photoelectron spectroscopy, indicating possible change at the film-substrate interface.

This work was supported by the Joint Studies Program (No. 203, 2016-2017) of the Institute for Molecular Science.

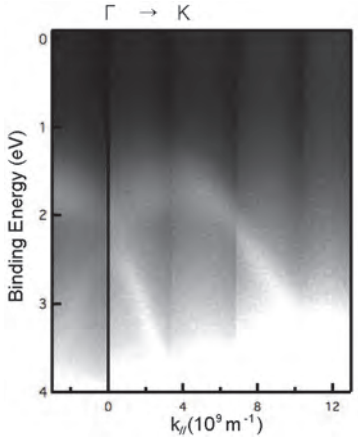

Fig. 1. ARPES spectra of GaSe thin film surface measured along Γ-K direction of GaSe(0001).

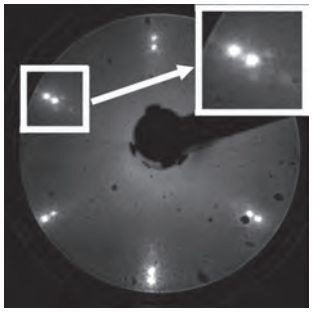

Fig. 2. LEED pattern of GaSe/Ge(111) sample surface showing spots corresponding to Moiré.

[1] B. Radisavijevic *et al*., Nat. Nanotechnol. **6** (2011) 147.
[2] A. Fleurence *et al*., Phys. Rev. Lett. **108** (2012) 245501.
[3] L. Plucinki *et al*., Phys. Rev. B **68** (2003) 125304.

BL6U

Epitaxial Silicene on h-BN Terminated ZrB_2 Thin Films

F. B. Wiggers[1], A. Fleurence[2], K. Aoyagi[2], T. Yonezawa[2], H. Yamane[3], Y. Yamada-Takamura[2], N. Kosugi[3], A. Y. Kovalgin[1] and M. P. de Jong[1]

[1] *MESA+ Institute for Nanotechnology, University of Twente, 7500 AE Enschede, The Netherlands*
[2] *Japan Advanced Institute of Science and Technology, School of Materials Science, Nomi 923-1292, Japan*
[3] *Department of Photo-Molecular Science, Institute for Molecular Science, Okazaki 444-8585, Japan*

Silicene is the silicon analogue of graphene, i.e. a two-dimensional (2D) silicon allotrope featuring an atomically buckled honeycomb-lattice. Theory predicts Dirac electrons and an electrically tunable spin-orbit bandgap of a few meV, leading to the topological quantum spin Hall phase [1]. However, these properties of free-standing silicene remain hypothetical, because so far only epitaxial silicene has been synthesized on metallic substrates such as Ag(111) [2], ZrB_2(0001) [3], Ir(111) [4], and ZrC(0001) [5], introducing non-negligible hybridization of electronic states and denying direct electrical characterization without complex processing.

The synthesis of silicene on insulating, weakly interacting substrates is therefore highly desired. Motivated by this, we studied the growth and properties of 2D silicon layers grown on the h-BN(0001)-terminated surface of a ZrB_2(0001) thin film on a Si(111) substrate. The h-BN terminated substrates were prepared ex-situ using plasma nitridation and annealing of epitaxial ZrB_2 films. Surface cleaning was performed at BL6U prior to silicene growth using annealing at about 800 °C to remove oxides. Silicon was deposited in steps by heating a Si strip by direct current. The resulting highly ordered 2D silicon layer on the h-BN terminated ZrB_2 surface was studied by LEED, ARPES, and core level PES.

It was found that the electronic structure of the so-obtained Si layer is very similar to that of epitaxial silicene on ZrB_2, which has been characterized previously [3]. Figure 1 shows the valence band structure as determined by ARPES measurements recorded with a photon energy of 50.5 eV. Besides ZrB_2 derived bands, characteristic Si-related bands can be identified centered around the K-point of the Si lattice, the most prominent of which is indicated by the dotted line. This particular electronic structure is virtually identical to that of silicene on ZrB_2, strongly suggesting that intercalation underneath the h-BN layer takes place. This conclusion is further supported by the Si 2*p* spectra (not shown). Interestingly, the h-BN layer has a negligible effect on the electronic structure of the silicene that it covers. This is promising for non-destructive capping of silicene, which is required for any analysis or application of silicene outside ultra-high vacuum.

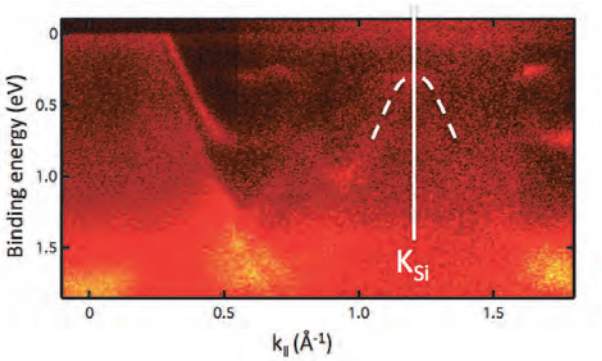

Fig. 1. ARPES spectra measured along the Γ-K direction of the 2D Si layer.

[1] M. Ezawa, New J. Phys. **14** (2012) 33003.
[2] P. Vogt, P. De Padova, C. Quaresima, J. Avila, E. Frantzeskakis, M. C. Asensio, A. Resta, B. Ealet and G. Le Lay, Phys. Rev. Lett. **108** (2012) 155501.
[3] A. Fleurence, R. Friedlein, T. Ozaki, H. Kawai, Y. Wang and Y. Yamada-Takamura, Phys. Rev. Lett. **108** (2012) 245501.
[4] L. Meng, Y. Wang, L. Zhang, S. Du, R. Wu, L. Li, Y. Zhang, G. Li, H. Zhou, W. A. Hofer and H.-J. Gao, Nano Lett. **13** (2013) 685.
[5] T. Aizawa, S. Suehara and S. Otani, J. Phys. Chem. C **118** (2014) 23049.

BL6U

Electronic Structure of Iron Phthalocyanine (I): Temperature-Dependent Interface-Specific Electronic State in Monolayer on Au(111)

H. Yamane[1, 2], A. Carlier[1, 3] and N. Kosugi[1, 2]
[1]*Institute for Molecular Science, Okazaki 444-8585, Japan*
[2]*The Graduate University for Advanced Studies (SOKENDAI), Okazaki 444-8585, Japan*
[3]*Department of Physics, University of Namur, Namur B-5000, Belgium*

Iron phthalocyanine (FePc) is well known as one of important organic semiconductors with unique electronic and magnetic properties. Among them, it was found that FePc molecule on Au(111) exhibits unique Kondo effects depending strongly on the adsorption configuration, e.g., ontop site at 2.6±1.4 K and bridge site at 110~150 K [1]. In the present work, in order to investigate the change in the electronic structure introduced by the Kondo effect, we have applied angle-resolved photoemission spectroscopy (ARPES) to the FePc monolayer on Au(111).

The experiment was performed at the in-vacuum undulator beamline BL6U. The clean Au(111) surface was obtained by the repeated cycles of the Ar^+ sputtering and the subsequent annealing at 700 K, as confirmed by the low-energy electron diffraction (LEED) and the Shockley state in ARPES. The ordered monolayer was obtained by flashing the FePc thin multilayer on Au(111) at 470 K.

Figure 1 shows the photoemission angle (θ) dependence of the ARPES spectra measured for the FePc monolayer on highly oriented pyrolytic graphite (HOPG) and on Au(111) at 20 K using hv = 45 eV. At the FePc/HOPG interface, the C 2*p*- and Fe 3*d*-derived peaks appear at the binding energy of 1.2 eV and 1.5 eV, respectively. The large background observed at θ = 30° originates from the π band of HOPG. The Fe 3*d* intensity is getting stronger than the C 2*p* intensity when $h\nu$ > 60 eV (not shown) as observed for the gas phase [2]. On the other hand, at the FePc/Au(111) interface, the C 2*p* peak at 0.7 eV exhibits the clear θ dependence with the intensity maximum at θ = 32° ($\boldsymbol{k} \approx 1.7$ Å^{-1}), while no clear Fe 3*d*-derived peaks appear below the C 2*p*-derived peak, as observed at the CoPc/Au(111) interface [3], indicating the modification of the Fe 3*d* orbital with the Au(111) surface. It is worthy of note here that a quite weak peak is appeared below the Fermi level (E_F) but is not observed at the clean Au(111) surface.

Figure 2 (a) shows the temperature dependence of ARPES at $\boldsymbol{k} \approx 1.7$ Å^{-1} for the FePc/Au(111) interface. With decreasing the temperature, the Fermi edge is getting sharpened and the interface-specific peak at 0.12 eV is getting visible. The difference ARPES spectrum between 30 K and 240 K shown in Fig. 2 (b) indicates the presence of the temperature-dependent interface states at 0 eV and 0.12 eV, which disappear at *ca.* 160 K. The increase in the density of states at E_F is the indication of the Kondo resonance, as reported in Ref. [1], which may also introduce the formation of the interface state observed at 0.12 eV.

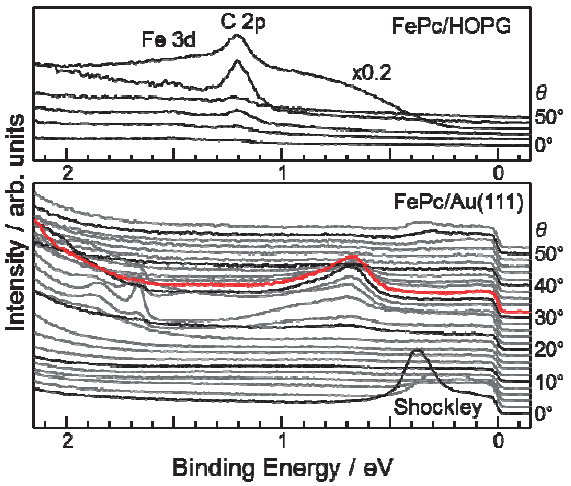

Fig. 1. Photoemission angle (θ) dependence of ARPES ($h\nu$ = 45 eV) measured for the interfaces of FePc/HOPG and FePc/Au(111) at 20 K.

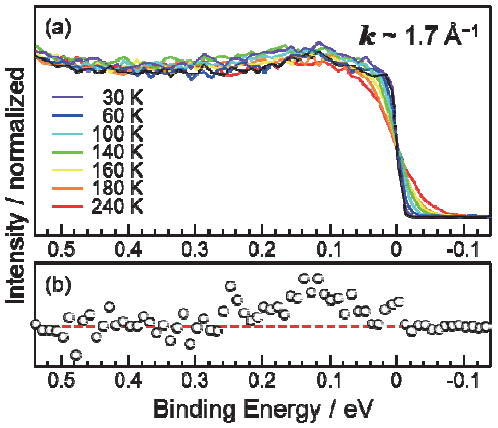

Fig. 2. (a) Temperature dependence of ARPES at $\boldsymbol{k} \approx 1.7$ Å^{-1} measured for the FePc/Au(111) interface. (b) Difference spectrum between 30 K and 240 K, which is obtained after the substrate-background subtraction and the smoothing.

[1] E. Minamitani *et al.*, Phys. Rev. Lett. **109** (2012) 086602.
[2] B. Brena *et al.*, J. Chem. Phys. **134** (2011) 074312.
[3] H. Yamane and N. Kosugi, J. Phys. Chem. C **120** (2016) 24307.

BL6U

Electronic Structure of Iron Phthalocyanine (II): Intermolecular Electronic Band Dispersion in Crystalline Multilayer

H. Yamane[1, 2], A. Carlier[1, 3] and N. Kosugi[1, 2]
[1]*Institute for Molecular Science, Okazaki 444-8585, Japan*
[2]*The Graduate University for Advanced Studies (SOKENDAI), Okazaki 444-8585, Japan*
[3]*Department of Physics, University of Namur, Namur B-5000, Belgium*

The intermolecular electronic band dispersion, originating from the periodicity of the molecular stacking structure, is essential to investigate the charge transport mechanism related to organic electronics. Recently, we have succeeded in precise observation of the quite weak intermolecular band dispersion for crystalline films of phthalocyanines [MPc, M = metal or H_2 (metal free)], such as MnPc, CoPc, ZnPc, F_{16}ZnPc and H_2Pc, by angle-resolved photoemission spectroscopy (ARPES) [1]. In this work, we have investigated the intermolecular band dispersion of the FePc crystalline film, which is difficult to observe precisely with respect to the other MPc films since the C 2*p* and Fe 3*d* energies are close to each other.

The experiment was performed at the in-vacuum undulator beamline BL6U. The cleanliness of the Au(111) surface was confirmed by the low-energy electron diffraction (LEED) and the Shockley state in ARPES, as obtained from the repeated cycles of the Ar^+ sputtering and the subsequent annealing at 700 K. The FePc multilayer is obtained by the vacuum deposition of purified FePc molecules onto the Au(111) as kept at 350 K.

Figure 1 shows the incident angle (α) dependence of N K-edge X-ray absorption spectra for the 300-Å-thick FePc films on Au(111). The sharp $1s \rightarrow \pi^*$ transition peaks appear at $h\nu$ = 398-405 eV. These peaks are strongest at grazing incidence (α = 70°) and are getting weaker with decreasing α, except for peak X at 399 eV due to the hybridization with Fe 3*d* orbital. Other broad $1s \rightarrow \sigma^*$ transition features ($h\nu$ > 405 eV) show the opposite polarization dependence. Furthermore, the FePc multilayer shows the clear LEED pattern as shown in the inset of Fig. 2. These evidences indicate that the FePc molecules on Au(111) form the flat- lying ($\beta \approx 0°$) crystalline film.

Figure 2 shows the photon energy ($h\nu$) dependence of the normal-emission ARPES spectra for the FePc crystalline film. Since the FePc crystalline film on Au(111) shows a Stranski-Krastanov growth mode, there are remanent substrate signals such as the Fermi edge, which we used for the fine $h\nu$ calibration. The topmost peak exhibits two components derived from the C 2*p* and Fe 3*d* orbitals as labeled in Fig. 2. The relative peak intensity between C 2*p* and Fe 3*d* is dependent on $h\nu$, which is slightly different from the case in the gas-phase FePc [2]. This difference can be ascribed to the weak intermolecular orbital overlap between C 2*p* and Fe 3*d*.

The C 2*p* peak shows a dispersive behavior with $h\nu$, while the Fe 3*d*-derived peak does not show such a behavior. This indicates the presence of the relatively strong intermolecular π-π interaction with the transfer integral of 25-30 meV and the localization of the Fe 3*d*-derived electronic state. The detailed lineshape analysis of the ARPES peak for the energy-*versus*-wavevector relation is now in progress.

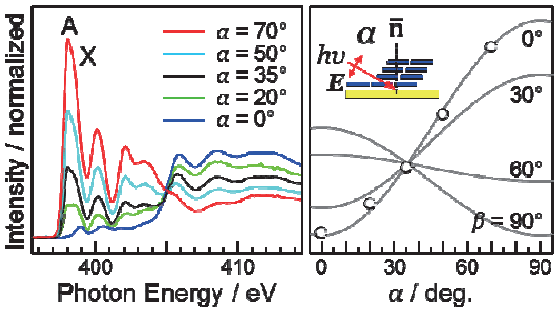

Fig. 1. Incident angle (α) dependence of N K-edge X-ray absorption spectra and the intensity plot of peak A for the FePc crystalline film at 20 K.

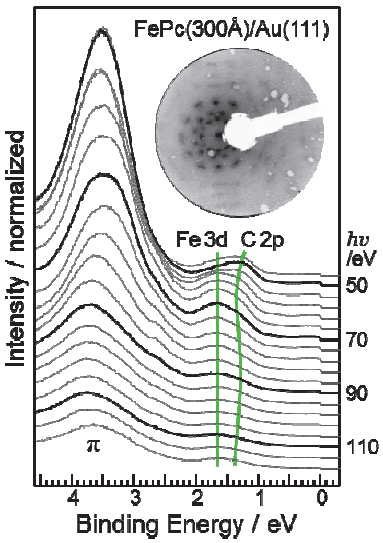

Fig. 2. $h\nu$-dependent ARPES spectra at the normal emission and the LEED image (E = 60 eV) for the FePc crystalline film at 20 K.

[1] H. Yamane and N. Kosugi, Phys. Rev. Lett. **111** (2013) 086602.
[2] B. Brena *et al.*, J. Chem. Phys. **134** (2011) 074312.

BL6U

Large Intermolecular π-Band Dispersion in Crystalline Films of Hexa-Peri-Hexabenzocoronene on Graphite(0001)

H. Yamane[1, 2] and N. Kosugi[1, 2]
[1]*Institute for Molecular Science, Okazaki 444-8585, Japan*
[2]*The Graduate University for Advanced Studies (SOKENDAI), Okazaki 444-8585, Japan*

Polycyclic aromatic hydrocarbons, e.g., hexa-*peri*-hexabenzocoronene (HBC) used in the present work, have attracted attention as a fragment of graphene. It has been reported that the HBC films on a highly oriented pyrolytic graphite (HOPG) exhibit a new substrate-induced polymorph, where all molecules adopt a recumbent orientation with planar π-stacking [1]. In the present work, we have investigated the presence of the intermolecular π-band dispersion in the HBC multilayer grown on a single crystalline graphite(0001) surface by means of angle-resolved photoemission spectroscopy (ARPES).

The experiment was performed at the in-vacuum undulator beamline BL6U. The single crystalline graphite(0001) surface was obtained by heating the nitrogen-doped 6H-SiC(0001) wafer based on the stepwise surface treatment [2]. The crystallinity of the graphite(0001) surface was confirmed by the low-energy electron diffraction (LEED).

The LEED image of the 250-Å-thick HBC crystalline multilayer on graphite(0001), displayed in the inset of Fig. 1, shows a sharp diffraction pattern, together with the incident-energy-dependent multiple scattering spots. We found that the diffraction pattern of the HBC multilayer agrees well with that of the HBC monolayer (not shown), and that the multiple scattering spots are not observable in the HBC monolayer, indicating the highly-ordered layer-by-layer growth of the HBC molecules on graphite(0001).

Figure 1 shows the photon energy (*hv*) dependence of the normal-emission ARPES spectra measured for the HBC multilayer on graphite(0001) at 20 K and 300 K. At 20K, the topmost valence band shows a large dispersion as 220 meV with *hv*. This dispersion is observable even at 300 K, indicating the presence of the stable and strong intermolecular π-stacking.

Figure 2 shows the energy-*vs*.-wavevector (*E*-***k***) map of the HBC multilayer on graphite(0001) at 20 K, which is obtained from the second-derivative curves of the normal-emission ARPES spectra in Fig. 1. The dispersion periodicity gives the intermolecular distance a = 3.369 Å, which is slightly larger than that of the graphite (a = 3.335 Å). The tight-binding fitting to the topmost band dispersion gives the intermolecular transfer integral t = 55 meV. Similar evidence is observable for the case of the HOPG substrate (not shown).

The present observation clearly indicates that the band-like hole transport can be realized in the new polymorphs of HBC on graphite.

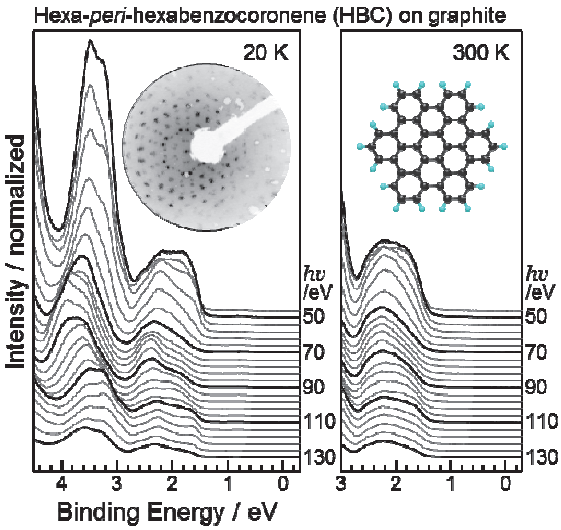

Fig. 1. Photon energy dependence of the normal-emission ARPES spectra for the HBC multilayer on graphite(0001) at 20 K and 300 K. The LEED image measured at E = 40 eV is show in the inset.

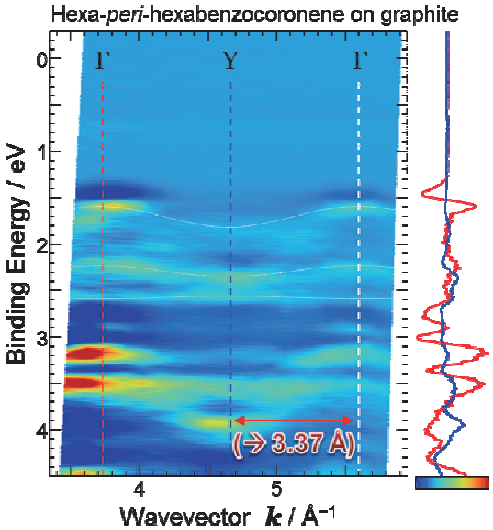

Fig. 2. *E*-***k*** map of the HBC multilayer on graphite (0001) at 20 K, obtained from the second derivatives of the normal-emission ARPES data. For the ***k*** conversion, we used the inner potential V_0 as −3.0 eV.

[1] P. Beyer *et al.*, ACS Appl. Mater. Interfaces **6** (2014) 21484.
[2] I. Forbeaux, J.-M. Themlin and J.-M. Debever, Phys. Rev. B **58** (1998) 16396.

BL6U

Origin of the Interface State at the Tetraphenyldibenzoperiflanthene Monolayer on Ag(111)

R. Shiraishi[1, 2], K. Yonezawa[2], T. Yamaguchi[1, 2], T. Ueba[1, 2], H. Yamane[1, 2], N. Kosugi[1, 2] and S. Kera[1, 2]

[1]*The Graduate University for Advanced Studies (SOKENDAI), Okazaki 444-8585, Japan*
[2]*Department of Photomolecular Science, Institute of Molecular Science, Okazaki 444-8585, Japan*

Strong modification of the electronic property in π-conjugated molecules adsorbed on a metal substrate has been reported, for example, 2D band dispersion, Kondo effect, and so on. These phenomena are induced by the hybridization of the electronic wave function between the molecule and the metal surface. Thus, the formation mechanism of the interface state has attracted attention for a long time.

Tetraphenyldibenzoperiflanthene (DBP, Fig. 1 (a)) is an interesting molecule for investigating the hybridized state between molecule and metal surface, because the molecule is lying-flat on the substrate and its large π-conjugated plane is expected to be far apart from the surface due to its phenyl rings. We reported DBP forms a well-ordered monolayer (ML) film on Ag(111) [1]. Here the interfacial electronic state of DBP(ML)/Ag(111) is investigated by angle-resolved ultraviolet photoelectron spectroscopy (ARUPS).

As shown in Fig. 1 (b), while UPS spectra of the gas phase and the ML film on HOPG show similar features due to weak interaction, the ML on Ag(111) shows the shift and broadening of these features. Moreover, no significant feature around the Fermi level and an additional feature at 1.4 eV are detected for DBP/Ag (111). The secondary cut-off of the DBP ML becomes lower by 0.8–1.0 eV than that of a clean Ag(111). The *negative* shift is more significant than that due to electron push-back effect of Xe/Ag (~0.5 eV) [2]. In general, hybridized states in many organic/metal systems appear as the filled LUMO. However, this assumption is hardly applicable to the case of DBP/Ag (111), because the electron transfer from the substrate to the LUMO would contribute *positive* surface potential shift. Therefore we concluded that these interface states (I_1-I_4) are caused by a hybridization between DBP and Ag(111) , hence the HOMO region is largely affected to give bonding and antibonding features of I_1 and I_2. The features I_3 and I_4 are described to HOMO-1(-2) and HOMO-3(-4) derived states, respectively.

This conclusion is further confirmed by the comparison of photoelectron angular distribution (PAD) between experiment and simulation [3]. In Fig. 1 (c) left, the azimuthal dependence of the I_1 and I_2 region is shown. Fig. 1 (d) shows the calculated PAD for HOMO and LUMO of a free molecule by multiple scattering theory. In Fig. 1 (c) right, the experimental intensities of I_1 and I_2 are compared to the theoretical simulations of HOMO and LUMO taken from Fig. 1 (d). The experimental pattern of I_1 (blue circle) well agrees with the simulation of the HOMO (black line), rather than that of the LUMO (red line). A deviation of experimental data from the simulation might reflect a spatial modulation of the HOMO due to the hybridization with the substrate band which is not taken into account for the present calculation.

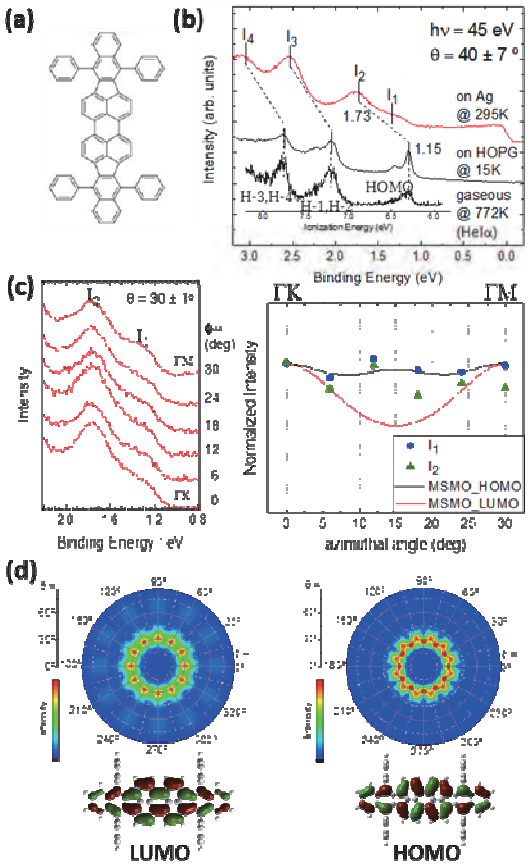

Fig. 1. (a) Chemical structure of DBP. (b) UPS of gaseous DBP (bottom), ML on graphite (middle), and ML on Ag(111) (top). (c) azimuthal ARUPS (left) and a comparison between experimental and theoretical pattern of HOMO and LUMO. All the intensity were normalized at φ = 0° for comparison. (d) PAD simulation of HOMO/LUMO for an isolated DBP. Two differently oriented molecules in a unit cell [1] and the (111) surface symmetry were considered.

[1] T. Kirchhuebel *et al.,* Langmuir **32** (2016) 1981.
[2] K. Wandelt *et al.,* Surf. Interf. Anal. **12** (1988) 15.
[3] S. Nagamatsu *et al*., e-J. Surf. Sci. Nano. **3** (2005) 461.

BL7U

On the Long-wavelength Approximation in the Photoelectric Effect

Y. Ishida[1], S. Ideta[2], K. Tanaka[2] and S. Shin[1]
[1]*ISSP, University of Tokyo, Chiba 444-8585, Japan*
[2]*UVSOR, Institute for Molecular Science, Okazaki 444-8585, Japan*

A long-wavelength approximation is often assumed *a priori* when the interaction between light and matter is concerned. The assumption, however, may be strongly invalidated in the surface region at the atomic scale particularly when the photon energy is low [1]. Here, we test the validity of the assumption in the photoelectric effect.

When the long-wavelength approximation is valid, the electrons subjected to the photon field $\boldsymbol{A}$ cannot sense the direction of the light propagation. The validity can thus be tested by investigating whether or not the angular distribution of photoelectrons depends on the direction of the incident light. Figure 1 (a) shows the setup for the test. The incident light is *s*-polarized, and the angular distribution of the photoelectrons are investigate by the analyzer [2]. In this configuration, it is only the direction of the light that breaks the mirror symmetry of the setup with respect to the plane spanned by the *s*-polarization vector and surface normal of the sample. The photoelectron distribution thus becomes asymmetric (symmetric) with respect to the geometrical mirror plane when the photoelectric effect is susceptible (unsusceptible) to the propagation vector. Note, we adopt the scalar gauge.

In the setup, the following two conditions are also imposed on the sample side: (1) The sample should not break the mirror symmetry of the geometry; (2) Near the surface Γ point, the sample has to have surface localized states, because they can strongly overlap to the photon field in the surface region that is under investigation. To this end, we chose highly-oriented Bi microcrystals grown on a highly-oriented pyro-graphite for the sample [3]. The Bi microcrystals are randomly oriented in plane with their 111 face oriented normal to surface, so that the effect of the crystal symmetry is averaged out in the azimuth. In other words, the sample has a high symmetry of C_∞. In addition, Bi(111) harbors Rashba-split surface states around the surface Γ point.

Figure 1 (a) shows the angular distribution of photoelectrons $I(E_B, \alpha)$ emitted from the highly-oriented Bi(111) microcrystalline thin film with the incidence of 17 eV light. Here, E_B and α are the binding energy and the emission angle, respectively. Clear dispersions are observed: The structures in [~0.1, 0 eV] are mainly due to the Rashba-split surface states. In order to investigate whether the distribution is symmetric about $\alpha = 0$, we show in Figure 2 (b) $\Delta_{sym}(E_B, \alpha) \equiv I(E_B, \alpha) - I(E_B, -\alpha)$. We observe some asymmetric distributions from the photoelectrons emitted from the Rashba bands, as well as those from the states occurring below 0.3 eV. Thus, the photoelectron distribution senses the direction of the incident light.

Based on the jellium model, the breakdown occurs only for *p*-polarized component of $\boldsymbol{A}$ [1]. The present results indicating that the approximation is broken even in the *s*-polarized case thus calls for a description beyond. We note that the three-slab model often used in the field of surface nonlinear optics can qualitatively explicate the phenomena.

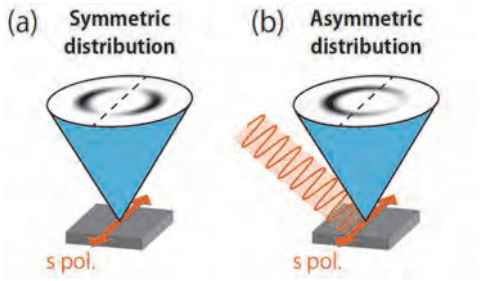

Fig. 1. Experimental geometry for testing the long-wavelength approximation in the photoelectric effect. When the long-wavelength approximation is valid, a mirror-symmetric photoelectron distribution is expected (a); if not valid, or when the direction of the incident light matters, the angular distribution becomes asymmetric (b).

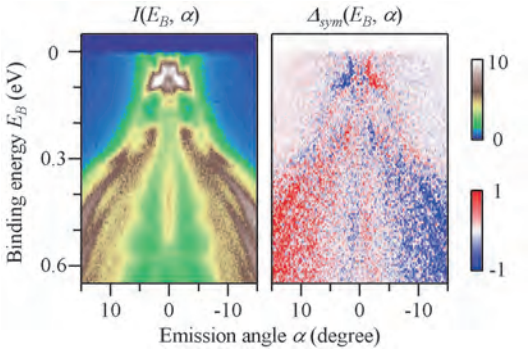

Fig. 2. Angular distribution of photoelectrons from highly-oriented Bi(111) thin film (a) and the asymmetry in the distribution (b).

[1] H. J. Levinson, E. W. Plummer and P. J. Feibelman, Phys. Rev. Lett. **43** (1970) 952.
[2] S. Kimura *et al.*, Rev. Sci. Instrum. **81** (2010) 053104.
[3] Y. Ishida *et al.*, Rev. Sci. Instrum. **87** (2016) 123902.

BL7U

Interfacial Interaction between Coronene Thin Film and Graphite

T. Yamaguchi[1, 2], T. Ueba[1, 2], M. Meissner[2], K. Yonezawa[2], R. Shiraishi[1, 2], S. Ideta[1, 2], K. Tanaka[1, 2] and S. Kera[1, 2]

[1] *The Graduate University for Advanced Studies (SOKENDAI), Okazaki 444-8585, Japan*
[2] *Institute for molecular science, Okazaki 444-8585, Japan*

Interactions between organic thin films and solid surfaces strongly affect the electronic structure at the interface which contributes to the performance of organic-based devices. Tanaka *et al.* observed a replica of a π-band of the highly oriented pyrolytic graphite (HOPG) surface appearing at the Γ-point below a critical temperature of 29 K [1]. The intensity of the replica band is enhanced at a low-energy photon ($h\nu \approx 11.5$ eV), indicating that the transition occurs resonantly via unoccupied states at 11.5 eV above the Fermi level. The authors suggested that the origin of the band is a superstructure due to surface defects, a charge density wave transition, or the adsorption of residual gas molecules [1, 2]. We observed similar replica bands for a coronene thin film on HOPG which, however, differ in the critical temperature and the resonance energy.

A clean surface of HOPG was obtained by cleaving in air and subsequent annealing in UHV. Coronene was purified twice by sublimation. The sample preparation was performed in a custom UHV chamber designed for organic molecules, with a base pressure of 2×10^{-7} Pa. A coronene layer with a nominal thickness of 2.5 Å was deposited at room temperature (RT) at a rate of 1 Å/min.

Figures 1 (a) and 1 (b) depict temperature dependences of $E(k)$ intensity maps at RT and 50 K. Fig. 1 (c) shows energy distribution curves (EDCs) derived from the $E(k)$ images. In Fig. 1 (b), the replica bands appear not only at the Γ-point as in the case of the pristine HOPG but also at 0.63 Å^{-1}, 1.11 Å^{-1}, and 1.26 Å^{-1} (not shown). Upon cooling, the shape of the highest occupied molecular orbital (HOMO) is markedly changed, namely the intensity decreases and the energy is higher by 60 meV as shown in Fig. 1 (c). The $h\nu$ dependence of the intensity at the Γ-point around the Fermi level is shown in Fig. 1 (d). An intensity maximum is observed at 12.8 eV, which is clearly different from the case of pristine HOPG, indicating a strong modification of the unoccupied state due to weak hybridization at the interface.

We observed similar multi-replica bands below 180 K. The critical temperature of 180 K is much higher than that of the pristine HOPG. The coronene molecules form a superstructure on HOPG at RT [3], however, there is no clear features of the replica band at RT, which may be smeared out by nuclear motions and/or weak wavefunction overlap. The occupied and unoccupied states are strongly modified by the weak interaction at the physisorbed interface nontrivial way and the impact may possibly enhanced at low temperature due to larger wavefunction overlap. A gap-opening and a change in effective hole mass should occur due to the interaction. They may be observed by more precise experiments.

[1] S. Tanaka *et al.*, Phys. Rev. B **84** (2011) 121411.
[2] S. Tanaka *et al.*, private communications.
[3] K. Walzer *et al.*, Sur. Sci. **415** (1998) 37.

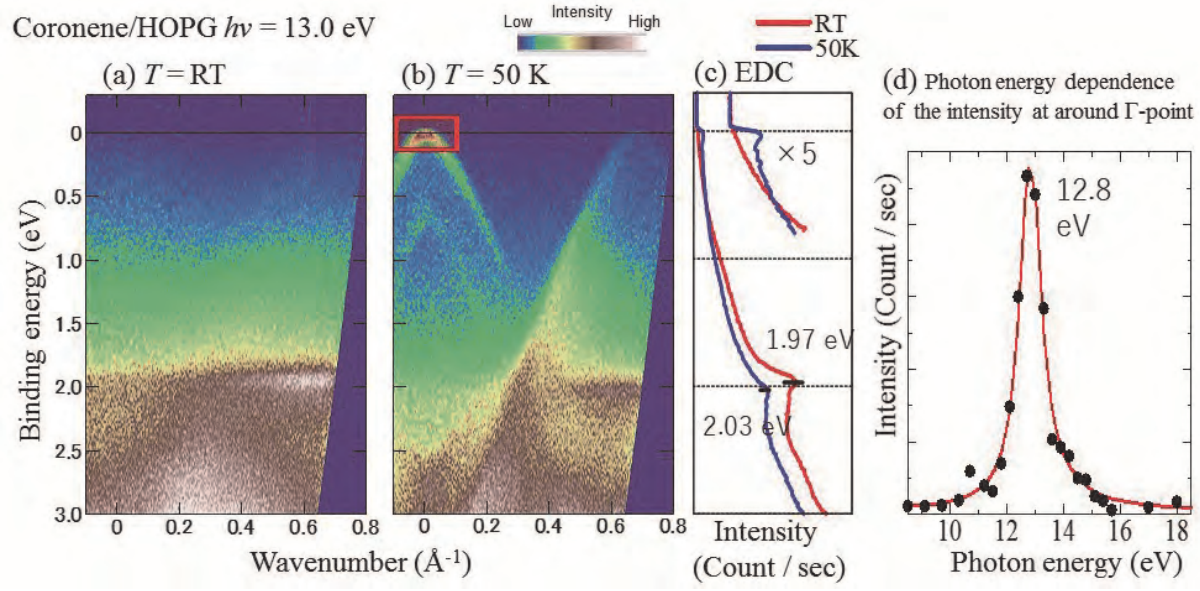

Fig. 1. $E(k)$ intensity maps of coronene/HOPG at (a) RT and (b) 50 K taken at 13.0 eV. (c) Momentum-integrated EDCs at RT (red) and 50 K (blue). (d) Intensity plot in red area in (b) as a fucnction of hv. The intensity of each energy is nomalized by photon flux. The red curve is a fitted curve using two Lorentzian functions.

UVSOR User 8